Global and Planetary Change 158 (2017) 83–102

Contents lists available at ScienceDirect

Global and Planetary Change

journal homepage: www.elsevier.com/locate/gloplacha

Miocene tectonic history of the Central Tauride intramontane basins, and the paleogeographic evolution of the Central Anatolian Plateau

Ayten Koç[a,*], Nuretdin Kaymakci[b], Douwe J.J. Van Hinsbergen[c], Klaudia F. Kuiper[d]

[a] Department of Geological Engineering, Van Yüzüncü Yıl University, Van 65080, Turkey
[b] Department of Geological Engineering, Middle East Technical University, Ankara 06531, Turkey
[c] Department of Earth Sciences, Utrecht University, 3508 TA Utrecht, The Netherlands
[d] Department of Earth Sciences, Vrije University of Amsterdam, De Boelelaan 1085, 1081 HV Amsterdam, The Netherlands

ARTICLE INFO

Keywords:
Ilgın Basin
Paleostress inversion
Central Taurides
Anatolia
Paleogeograph

ABSTRACT

Marine Lower-Upper Miocene deposits uplifted to > 2 km elevation in the Tauride mountains of southern Turkey are taken as evidence for the rise of a nascent plateau. The dynamic causes of this uplift are debated, but generally thought to be a regional dynamic topographic effect of slab motions or slab break-off. Immediately adjacent to the high Tauride mountains lie the Central Tauride Intramontane Basins, which consist of Miocene and younger fluvio-lacustrine basins, at much lower elevations than the highly uplifted marine Miocene rocks. These basins include the previously analyzed Altınapa and Yalvaç basins, as well as the until now undescribed Ilgın Basin.

In this paper, we aim to constrain the paleogeography of the Central Tauride Intramontane Basins and determine the role of the tectonics driving the formation of the high Miocene topography in southern Turkey. Therefore, we provide new data on the stratigraphy, sedimentology and structure of the continental Ilgın Basin. We provide an $^{40}Ar/^{39}Ar$ age of 11.61 ± 0.05 Ma for pumice deposits in the stratigraphy. We provide paleostress inversion analysis based on growth faults showing that the basin formed during multi-directional extension, with NE-SW to E-W dominating over subordinate N−S extension. We conclude that major, still-active normal faults like the Akşehir Fault also controlled Miocene Ilgın basin formation, with proximal facies close to the basin margins grading upwards and basinwards into lacustrine deposits representing the local depocenter. The Ilgın Basin was a local depocenter, but it may have connected with the adjacent Altınapa Basin during high lake levels in late Serravallian time. The Ilgın Basin and the other continental basins provide key constraints on the paleogeography and tectonic history of the region. These continental basins were likely close to the paleocoastline during the Late Miocene after which there must have been major differential uplift of the Taurides. We suggest that the extension we documented in the Central Tauride intramontane basins are in part responsible for the major topography that characterizes the Central Taurides today. The causes of extension remain engmatic, but we suggest that the tomographically imaged Antalya Slab may have caused the contemporaneous formation of NE-SW trending *syn*-contractional basins in the west and NW-SE trending Central Tauride intramontane basins in the east by slab retreat. Our study highlights that the Neogene deformation history, and perhabs even active tectonics, may be strongly affected by complex slab geometry in SW Turkey, and that crustal deformation plays an important role in generating the Miocene Tauride topography. The role of this crustal deformation needs to be taken into account in attempts to explain the ride of the Taurides and the evolution of the Anatolian Plateau.

1. Introduction

The Tauride mountains of southern Anatolia underwent spectacular uplift of > 2 km in the last ~8 Ma (Cosentino et al., 2012; Schildgen et al., 2012a, b; Cipollari et al., 2013). This uplift created the southern margin of the modern internally drained elevated region in central Anatolia known as the Central Anatolian Plateau (Lüdecke et al., 2013; Schemmel et al., 2013; Meijers et al., 2016). The most prominent example of highly risen marine sediments are found in the Mut basin that unconformably overlies the Upper Cretaceous-Paleogene Tauride fold-thrust belt (Fig. 1a and b), but also in the Central Taurides west of Beyşehir highly elevated marine sediments are found (Şenel, 2002, Schildgen et al., 2012a, b), while deep-marine Pliocene sediments are exposed in the Adana basin (Radeff et al., 2017). Because no intense

* Corresponding author.
E-mail address: aytenkoc@yyu.edu.tr (A. Koç).

http://dx.doi.org/10.1016/j.gloplacha.2017.09.001
Received 12 April 2017; Received in revised form 6 August 2017; Accepted 5 September 2017
Available online 07 September 2017
0921-8181/

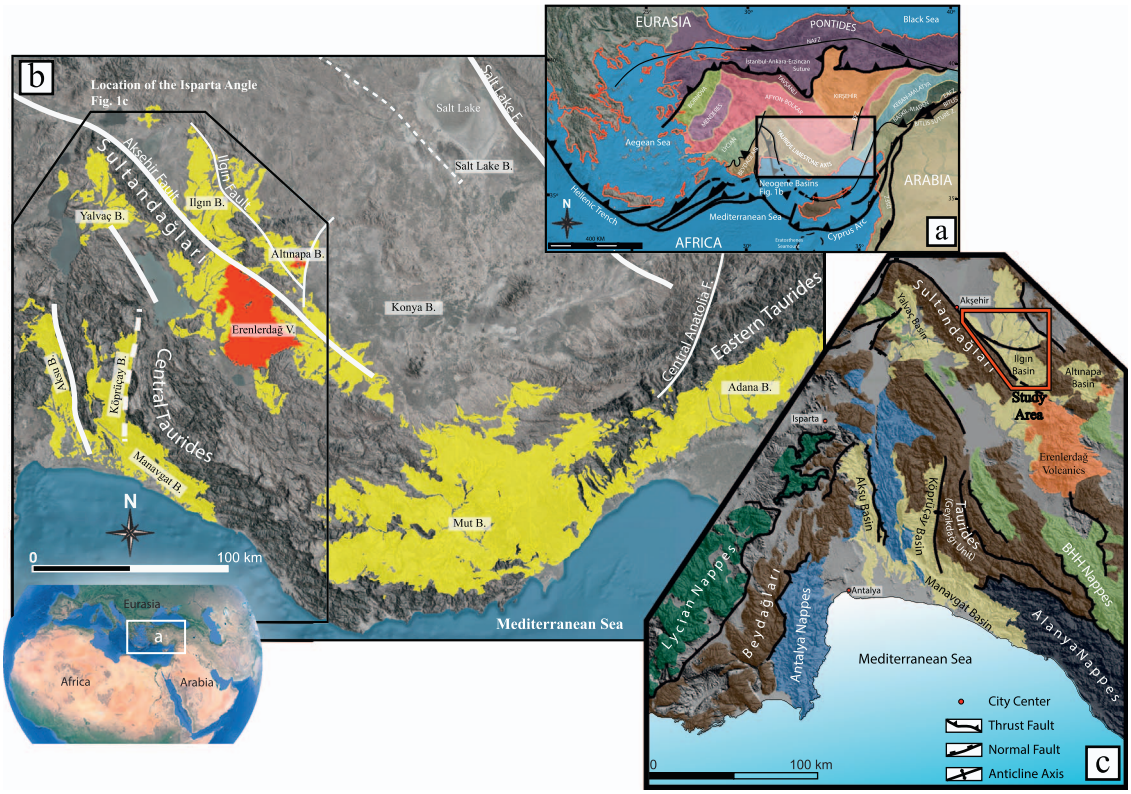

Fig. 1. (a) Simplified structural map and major tectonic zones of Turkey overlain on an SRTM topographic image. (b) Location of the Miocene basins (marine and continental) and major tectonic structures in the Central Anatolia (based on 1/500000 scale geological map (Ankara, Konya and Adana maps) produced by The Mineral Research and Exploration Directorate of Turkey (MTA)) (c) Simplified geological map of the Isparta Angle and location of the study area from 1/500000 scale geological map (Konya map) produced by The Mineral Research and Exploration Directorate of Turkey (MTA).

folding and thrusting of these Mio-Pliocene sediments has been recognized (e.g., Schildgen et al., 2012a, b; Fernández-Blanco, 2014), it is generally assumed that crustal deformation played no significant role in the rise of southern Anatolia. This rise is instead thought to be the result from a dynamic topographic response to processes in the underlying plate, such as slab break-off, slab segmentation, or mantle delamination (e.g., Schildgen et al., 2014; Bartol and Govers, 2014; Govers and Fichtner 2016).

Adjacent to the Central Taurides along the western limit of the Tuzgölü Basin (Fig. 1b), however, Miocene fluvio-lacustrine sediments and volcanics – here termed the Central Tauride Intramontane Basins – are exposed in a region with a current elevation of ~1000 m, i.e. > 1 km lower than the contemporaneous marine deposits exposed in the high Tauride mountains. For instance the elevations of Altınapa and Yalvaç basins (e.g., Koç et al., 2012, 2016a) (Fig. 1b and c) ranges around 1000–1250 m. This illustrates that the major uplift in southern Turkey is associated with the developement of differential relief on length scales of tens of kilometers. To understand which features must be explained by dynamic topographic responses to inferred mantle processes, it is key to decipher the role of crustal deformation in the recent uplift and resultant topography.

In this paper, we therefore analyse the paleogeography of the southern Central Anatolian Plateau. To that end, we here provide new constraints on the age, infill, and tectonic history of Ilgın Basin, which together with the Altınapa and Yalvaç basins hosts the best-exposed Miocene stratigraphic succession of the Central Tauride intramontane basins (Fig. 1b and c). We provide a new $^{40}Ar/^{39}Ar$ age of volcanic rocks in the basin. In addition, we show results from kinematic analysis combined with remote sensing and field mapping techniques, and are used to unravel tectonostratigraphical evolution of the basin and provide constraints on the spatio-temporal positions of paleoshorelines that prevailed during the Neogene on the southern margin of the Turkey.

2. Geological setting

The tectonic evolution of the Eastern Mediterranean region has been dominated since the Cretaceous by Africa-Eurasia convergence, which was accommodated by northward subduction of a complex paleogeographic mozaic of Neotethyan oceanic and Kırşehir-Tauride microcontinental lithosphere (Şengör and Yilmaz, 1981; Görür et al. 1984; Kaymakci et al. 2009; van Hinsbergen et al., 2016) (Fig. 1a). To the north, Neotethys subduction has been active beneath the Pontides along the southern Eurasian margin since the Jurassic (Okay et al., 2013; Dokuz et al., 2017). To the south, a second subduction zone formed in Late Cretaceous time below oceanic lithosphere, around 95 Ma, within which supra-subduction zone spreading centers formed upon subduction initiation that are now widely preserved as ophiolites that also overlie the Taurides (Yalınız and Göncüoğlu, 1998; Çelik et al., 2006; Kaymakci et al., 2009; Parlak et al., 2013; Parlak, 2016; van Hinsbergen et al., 2015, 2016; Gürer et al., 2016). Below these ophiolites, an overall foreland propagating fold-thrust belt formed that derived from a microcontinental domain that was separated by an ocean basin from Africa and Arabia. From this microcontinental domain, internal, crystalline units were accreted, including the Tavsanlı, Kırşehir, and Afyon zones (Pourteau et al. 2010, 2014; Plunder et al., 2015) (Fig. 1a), that accreted in Cretaceous time, and the external Tauride fold-thrust belt that accreted in Paleogene time (van Hinsbergen et al., 2016). The southern of these subduction zones is still active today., whereas the subduction zone below the Pontides stopped being active in central Turkey following the collision of the Kırşehir-Tauride nappe stack below the Cretaceous ophiolites with the Pontides starting in the latest Cretaceous (Kaymakci et al., 2009; Meijers et al., 2010).

The Taurides were separated in the south from Arabia and Africa by an oceanic branch of the Neotethys that closed north of the Arabian plate in Eastern Turkey along the Bitlis suture zone at the end of the

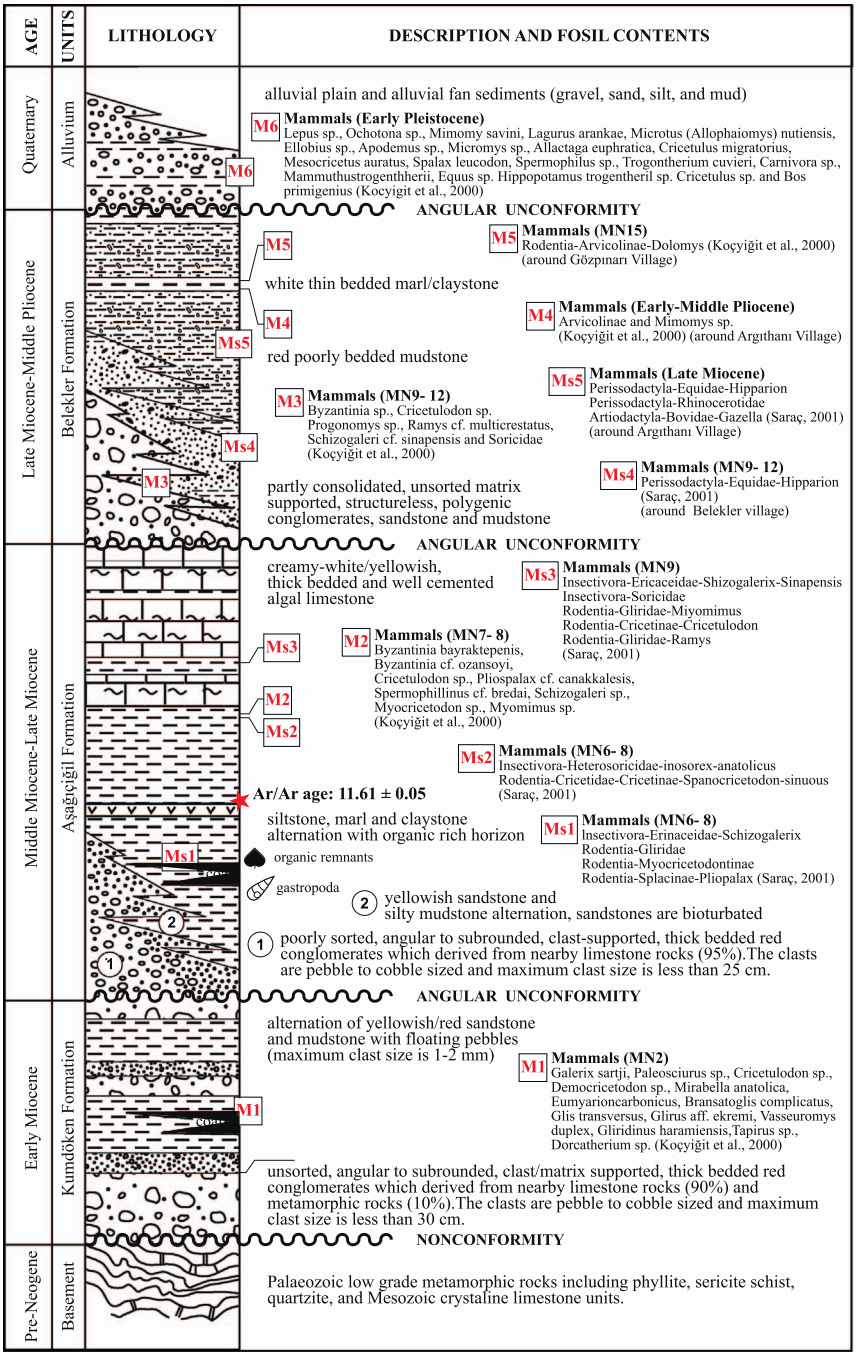

Fig. 2. Generalized stratigraphic column of the Ilgın Basin. Red labels with rectangle outline indicate the horizons of the fauna (mammalian fossils) and flora (spores and pollens). (For interpretation of the references to color in this figure legend, the reader is referred to the web version of this article.)

Middle Miocene (Şengör and Yilmaz, 1981; Yilmaz, 1993; Kaymakci et al., 2010), but still subducts today along the Cyprus subduction zone in the south (Khair and Tsokas, 1999; Granot, 2016). This active subduction zone is associated with slabs that were imaged by seismic tomography, which has been interpreted to show two separate slab segments below the central Taurides: 1) the Cyprus slab, a northwards dipping slab subducting at the Cyprus trench, which in most of the upper mantle can be tomographically discerned from 2) the Antalya slab (Koç et al., 2016a, 2016b; Biryol et al., 2011; van der Meer et al., 2017), an ENE-dipping, NNW–SSE striking slab with an associated Benioff zone (Kalyoncuoğlu et al., 2011) under the Central Taurides of which the surface connection is enigmatic (Biryol et al., 2011; Faccenna et al., 2006; Gans et al., 2009; van Hinsbergen et al., 2010b, Koç et al., 2016b; van der Meer et al., 2017).

The Tauride fold-thrust belt is presently exposed in the high Tauride axis, flanked and overlain by Neogene basins filled by marine to terrestrial sediments and in places volcanics (Fig. 1b). The dominantly marine basins are located mainly in the southern flank of the belt and include the Manavgat, Köprüçay, Aksu (collective these three basins are called as Antalya Basins), Mut and Adana basins all containing a Miocene (Burdigalian to Messinian) marine stratigraphy, in some cases (e.g. Adana and Aksu basins) reaching into the Lower Pliocene (Bassant et al., 2005; Çiner et al., 2008; Darbas and Nazik, 2010; Derman and Gürbüz, 2007; Eriş et al., 2005; Gül, 2007; Janson et al., 2010; Karabıyıkoğlu et al., 2005; Poisson et al., 2003; Yetiş, 1988; Schildgen et al., 2012a, b; Radeff et al., 2016, 2017) (Fig. 1b). To the north of the Taurides, intramontane continental basins including the Altınapa, Yalvaç and Ilgın basins formed during Neogene time (Fig. 1c) (Eren, 1993, 1996; Göğer and Kıral, 1969; Özcan et al., 1990; Özkan, 1998; Özkan and Söğüt, 1999; Yağmurlu, 1991a,b; Koç et al. 2012 and

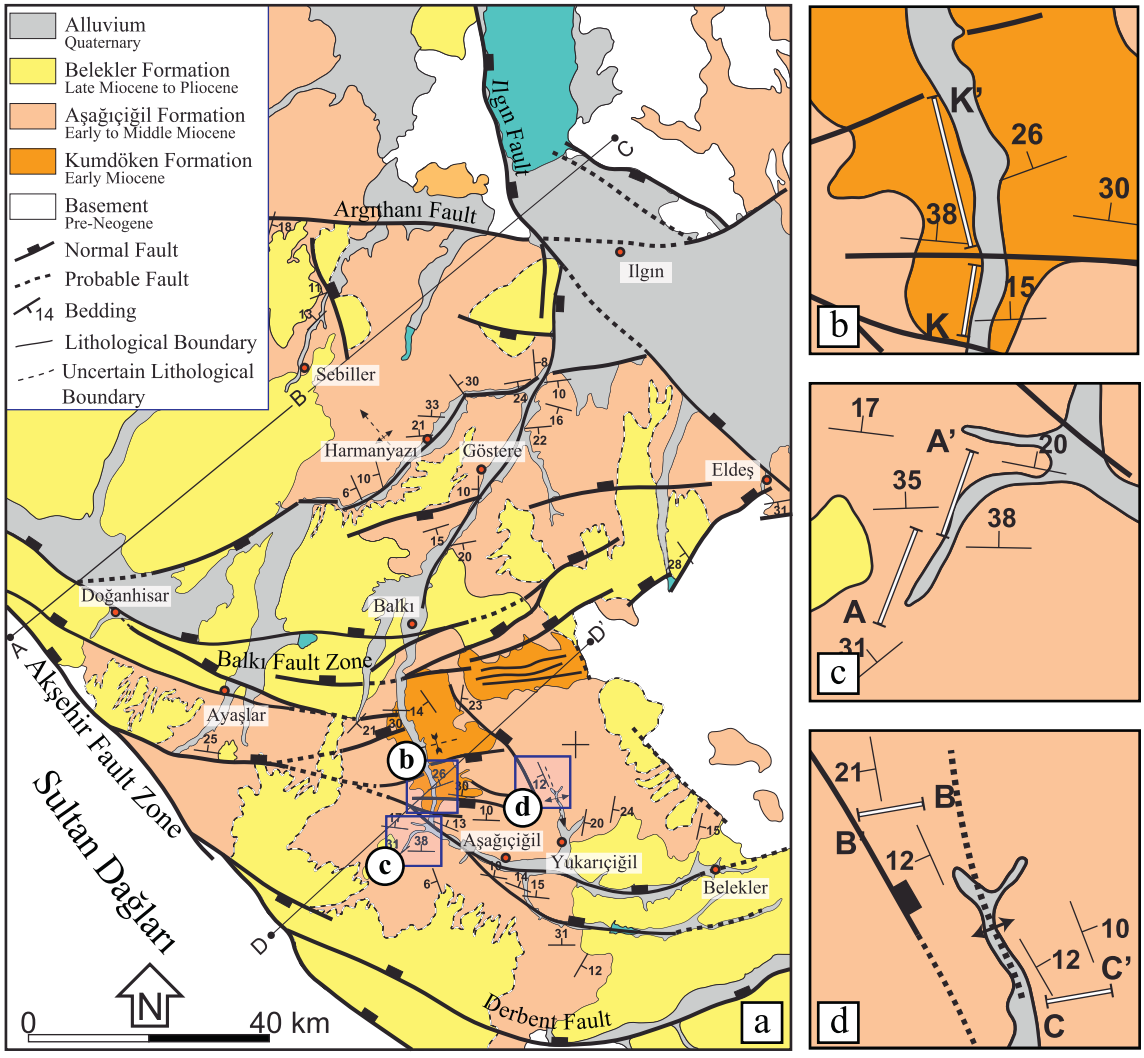

Fig. 3. The geological map of the Ilgın Basin from the 1/100000 scale geological map produced by The Mineral Research and Exploration Directorate of Turkey (MTA) is revised based on the field studies and remotely sensed data. Blue rectangle areas are used to indicate the location of the measured sections of the lithological units. Inset b for Aşağıçiğil formation (AcF), Inset c for Kumdöken formation and inset c for lacustrine part of the Aşağıçiğil formation. Routes of the measured sections are indicated by white solid lines (A-A′ for the Aşağıçiğil Formation, (K-K′) for the Kumdöken formation and (B-B′ and C-C′) lacustrine part of the Aşağıçiğil Formation. (For interpretation of the references to color in this figure legend, the reader is referred to the web version of this article.)

2016a). Koç et al. (2012; 2016) analyzed the tectono-stratigraphic evolution of the Altınapa and Yalvaç basins and claimed that these basins evolved under uniaxial stress regime which gave way to the multi-directional extension during the Middle (and perhaps Burdigalian) Miocene to Late Miocene. The Ilgın Basin, located to the north of the Altınapa basin (Fig. 1c) has not been studied in detail yet, and is characterized by thick accumulations of continental deposits and was developed on the metamorphosed Mesozoic carbonates of the Afyon zone that underwent high-pressure metamorphism during the latest Cretaceous to Paleocene (Özdamar et al., 2012; Özdamar et al., 2013, Pourteau et al., 2014) and that were extensionally exhumed until middle Eocene time. It is located in the present-day footwall of the seismically active Akşehir fault which has previously been interpreted as a thrust fault (Boray et al., 1985; Şaroğlu et al., 1987, Barka et al., 1995). However, recent studies including focal mechanism solutions, GPS studies, and outcrop observations clearly demonstrate that the Akşehir Fault is a normal fault with minor oblique-slip component that change depending on the location and fault orientation (Koçyiğit, 1984; Koçyiğit et al., 2000; Koçyiğit and Özacar, 2003; Aktuğ et al., 2010; Ergin et al., 2009). In this paper, we provide the first detailed account of its structural geology and expand the stratigraphic and sedimentological history of the basin.

3. Lithostratigraphy

The stratigraphy of the Ilgın Basin consists of continental clastic sediments. Lignite-rich levels are the best-studied deposits in the basin and the earliest studies (Lahn, 1945; Wedding, 1954; Bektimuroğlu, 1978) focused mainly on evaluating the lignite mining potential of the basin. The first study that incorporated the entire Neogene infill of the basin was performed by Tüfekçi (1987) in the northern part of the Ilgın Basin, who defined Neogene units based on geomorphological criteria, identifying one single formation with three members. After these pioneering studies, the Neogene stratigraphy of the Ilgın Basin was constructed by Koçyiğit et al. (2000), who provided additional age constraints from macro- and micro-mammalian fossils. They divided the Neogene deposits in the basin into three main lithostratigraphic units from older to younger; (1) the Köstere/Gölyaka formation, (2) the Doğancık/Gözpınarı formation and (3) the Taşköprü/Dursunlu formation. Hüseyinca and Eren (2007) provided the most recent study focused on the northern part of the Ilgın town and identified four formations, from older to younger including (1) the Harmanyazı formation, (2) the Ulumuhsine formation, (3) the Sebiller formation and (4) the Tekeler formation, which are not compatible with the previous subdivisions. Because we did not find the previous

subdivisions sufficient to describe the basin's evolution, and in keeping the stratigraphic divisions in the adjacent Altinapa basin, the lithostratigraphy of the Ilgın Basin is revised in this study and three main stratigraphic units are described, from older to younger including (1) the Kumdöken formation, (2) the Aşağıçiğil formation, and (3) the Belekler formation (Umut et al., 1987). Their lithology, age and contact relationships are described in the following sections and the first-order interpretation of their depositional environments is also provided (Fig. 2).

3.1. Kumdöken Formation

The Kumdöken formation is characterized by alternation of boulder to block sized reddish conglomerates with fine grained reddish/yellowish mudstone. In previous studies, it was regarded as a conglomerate member of the Aşağiçiğil formation (Koçyiğit et al., 2000, Hüseyinca and Eren 2007). We redefined the conglomerate member of Aşağıçiğil Formation as Kumdöken formation because of presence of unconformity and we mapped it as a separate formation. The base of the Kumdöken formation is mainly represented by conglomerates. Upwards, the conglomerates alternate with coarse to fine grained sandstone and silty-mudstone. These lithologies are well-exposed along the Ilgın-Beyşehir road (Fig. 3b), near Kumdöken, which is selected as the type locality. The contact relationship between the Kumdöken formation and the basement rocks is not well-exposed, but the Kumdöken formation is the oldest observable Neogene rock unit in the basin and the contact relationships between the Kumdöken formation and the basement rocks is probably a nonconformity. The formation is unconformably overlain by the Aşağıçiğil formation (Fig. 4a).

The oldest part of the sequence starts with generally clast-supported (or matrix supported at some levels), well-cemented and thick-bedded conglomerates that consist mostly of creamy white and dark/light gray recrystallized limestone (90%) and various cherts and rounded pebbles of low-grade, greenish metamorphic rocks (%10) set in a silty-sandy matrix with iron oxide cement (Fig. 5a). Clasts of the conglomerates are angular to sub-rounded, poorly sorted and ranging from gravel to boulder size (occasionally up to 25 cm of the long axis). A sedimentary structure such as pebble imbrication is occasionally observed at this level of the formation. Bottom bedding surfaces of the conglomerates are remarkably irregular with scour-and-fill structures (Fig. 5b). The unit is followed upwards by red to yellow sandstone and silty mudstone alternating with conglomerates. This thin- to medium-bedded (5–40 cm) silty-mudstone levels contain 2–3 mm coarse sands/granules that are floating in muddy matrix. The unit is followed upwards by channel structures consisting of coarse sand and gravel size clasts within mudstone levels. Additionally intense bioturbation (Fig. 5c) and cross-bedded structures are noted at higher levels in the sequence. The measured section of the Kumdöken formation, indicated as K-K′ in Fig. 3b has a minimum thickness of 375 m (see supplementary data).

Koçyiğit et al. (2000) reported micro-mammal fauna from different stratigraphic horizons of fluvio-lacustrine deposits which are located in the footwall of the Ilgın Fault. They reported following fauna north of Ilgın *Galerix sartji, Paleosciurus sp., Cricetulodon sp., Democricetodon sp., Mirabella anatolica, Eumyarioncarbonicus, Bransatoglis complicatus, Glis transversus, Glirus aff. Ekremi, Vasseuromys duplex, Gliridinus haramiensis, Tapirus sp., Dorcatherium sp.*, all characterizing mammal stage MN2 (M1 in Fig. 2) zone (Steininger, 1999; Mein, 1999). They named these units as Gölyaka formation and claimed that they are lateral equivalent of their Köstere formation in the Ilgın that contains rodent fossils indicating Middle to Late Miocene (MN 6–8 Zones). On the other hand, Krijgsman et al. (1996) who did a magnetostratigraphy of a continental section in the north of the Ilgın Basin, the Harami section. The *Eumyarion* and *Spano/Democricetodon* dominated assemblages of the Harami 1 and 3 localities are correlated to chrons C6Bn.2n (22.9 Ma) and C6Bn.1r (22.8 Ma), respectively, and are of early Miocene Age. Based on these data, the basal conglomeratic member of the Gölyaka formation of Koçyiğit et al. (2000) corresponds to Kumdöken formation and the MN 6–8 μ-mammal localities belongs to Aşağıçiğil formation in our stratigraphy. Therefore, the age of Kumdöken formation is estimated at Early Miocene.

Unsorted, angular and boulder-sized reddish conglomerates in the lower level of the unit indicates very close proximity to the source area. Sandy matrix-supported conglomerates indicate lower energy flow regime, the clast-supported conglomeratic levels indicate releatively high energy fluvial depositional environment where sand is carried in suspension (Colby 1963). The erosional base of the conglomerate units also demonstrates a high-energy environment. In the measured section of the Kumdöken formation, inversely graded conglomerates are also observed at some levels of the sequence. This type of grading is relatively uncommon, but is characteristic of debris flow deposits common in alluvial fan environments (Miall and Smith, 1989, Miall, 1996). The fine-grained red mudstones represent a quiet-water depositional environment. Red coloration of the mudstone reflects deposition in an oxidizing environment. This is generally achieved in continental environments due to oxidation (Walker, 1967). Therefore, the mudstones may be deposited in river floodplains, in downstream parts of the fluvial environment, or in distal parts of alluvial fans. The Kumdöken formation comprises facies associations ranging from alluvial fans to proximal fluvial systems of both axial deposition and tributaries entering the system laterally.

3.2. Aşağıçiğil Formation

The Aşağıçiğil Formation was named by Umut et al. (1987) and is characterized by alternation of white/yellowish and gray limestone, sandstone, tuff, marl and claystone. Alternative names were provided by Koçyiğit et al., (2000) who termed this the Köstere formation, and interpreted its depositional environment as a *syn*-tectonic fan to flood plain setting. Additionally, Hüseyinca and Eren (2007) defined it as the Harmanyazı formation characterized by claystone as a basic lithology intercalated with marl and limestone. The Aşağıçiğil formation is well-exposed along the Balkı-Aşağıçiğil main road, and two sections were measured to characterize the unit, close to the village of Aşağıçiğil (Fig. 3c and d). The Aşağıçiğil Formation unconformably overlies the Kumdöken formation in the south of the basin (Fig. 4a and b). It is delimited by the Akşehir Fault in the west, whereas in the east lacustrine algal limestones of the Aşağıçiğil Formation onlap over basement rocks, near Çavuşçugöl (Fig. 3). The Belekler formation unconformably delimits the upper boundary of the formation in the south and the north of the basin (Fig. 4c and d).

The lithology and facies characteristics of the unit are gradually changing from the west, which defines the tectonically active boundary of the basin, to the east which defines the depocenter of the basin. Based on the basin geometry, the first measured section (SC1) (see supplementary data) was recorded along the Kıreşen Stream, a branch of the Balkı River, close to the western edge of the basin (A-A' line in Fig. 3c). The sequence starts at the bottom with angular, poorly rounded, unsorted, both matrix and locally clast-supported gray/yellowish conglomerates (Fig. 5d). Clasts of the conglomerates ranging from pebble to cobble size (occasionally up to 25 cm), are polymict, and consist of 85% variable type and color (dark/light gray and creamy white) limestone, white quartz and greenish metamorphic rocks with slight foliation, and other rock fragments (15%). At these levels stratification is poor and the unit is irregularly bedded. The sequence continues upwards with sub-rounded, graded, clast-supported dark gray conglomerates alternating with yellowish, highly bioturbated and fresh water gastropod-bearing (Fig. 5e) pebbly sandstones. Pebble imbrication is occasionally observed at these conglomeratic levels. Channel lag deposits in this coarse sandstone are clast-supported and composed of coarse to medium size gravel. The coarse-grained sandstone grades upwards into silty sandstone. At the stratigraphically higher levels, the section shows alternation of marl, siltstone and organic-rich blue

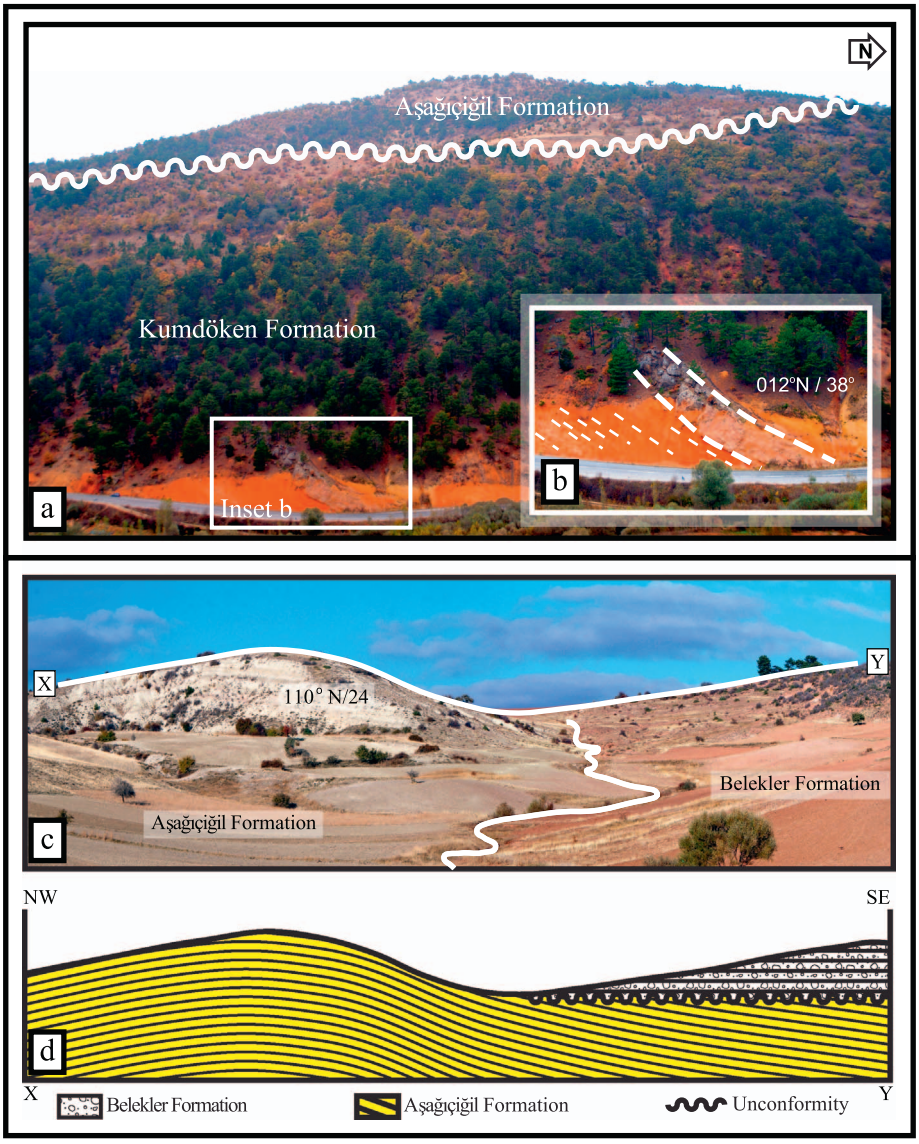

Fig. 4. (a) Field view of an angular unconformity between the Kumdöken and Aşağıçiğil formations. White rectangle indicated as inset b shows the bedding attitude of the Kumdöken formation in azimuth format. (b) Field view of an angular unconformity between between Aşağıçiğil and Belekler formations. The cross section direction is from NW to SE.

claystone, and finally medium to thick bedded algal limestone (Fig. 5f). The Aşağıçiğil Formation has a minimum thickness of 357 m in this section (SC1).

From the Sultandağları Mountain in the west towards the center of the basin, the second section was measured (see supplementary data). The section is located 2 km north of Yukarıçiğil (B-B′ in Fig. 3d) and is characterized by a lateral decrease in grain size. The facies changes into gray mudstone/white marl and algal limestone (Fig. 5g). The oldest part of the section starts with dark gray mudstone unit with thin pumice-bearing levels (Fig. 5h). From this level, a pumice sample was collected for $^{40}Ar/^{39}Ar$ dating. Aside from pumice levels, 10-15 cm thick organic-rich horizons also intercalate with mudstone/claystone units. At the base of the SC2, the Aşağıçiğil Formation juxtaposed along a fault with the Kumdöken formation. The upper boundary of the Aşağıçiğil Formation is clearly observed in the field, 2 km east of Yukarıçiğil, where the Belekler formation unconformably overlies the Aşağıçiğil Formation (Fig. 4c and d). The 63 m thick SC2 section represents a lateral equivalent of the (upper part of) SC1. A third section (SC3) (line C-C′, in Fig. 3d), equivalent of the SC2 was measured on the opposite flank of a broad anticline in that part of the basin. It is thicker than the SC2, with a thickness of approximately 130 m.

Koçyiğit et al. (2000) reported following vertebrate fossil assemblages including *Byzantinia bayraktepenis, Byzantinia* cf. *ozansoyi, Cricetulodon sp., Pliospalax* cf. *canakkalesis, Spermophillinus* cf. *bredai, Schizogalerix sp., Myocricetodon sp., Myomimus sp.,* which characterizes MN7–8 zone (M2 horizon in Fig. 2). Saraç (2001) also reported fossil vertebrates which indicate MN6–9 zone (Ms1, Ms2 and Ms3 in Fig. 2) from fluvio-lacustrine deposits corresponding to the upper part of the Aşağıçiğil Formation. In a palynological study performed by Karayiğit et al. (1999) lignite samples collected from three borehole cores drilled in the dry part of the Çavuşçu Lake in the hanging wall of the Ilgın Fault were collected. Acording to floral assemblages of the Ilgın lignite, a Middle Miocene age is assigned to this unit. Based on these findings, Middle to Late Miocene age is assigned for the Aşağıçiğil formation, which is constrained further by our $^{40}Ar/^{39}Ar$ age data discussed below (see Section 4).

Boulder to block-size, sub-angular to sub-rounded, matrix-supported conglomerates without any appreciable sedimentary structures (massive) and occasional reverse grading indicate alluvial fan or alluvial apron deposition (Miall, 1996). Angular/sub-rounded and clasts-supported conglomerates with sedimentary structures including pebble imbrication, channel lag deposits and normal graded bedding indicate fluvial environment. Moreover, presence of floating pebbles in the sandstones and an obviously water-laid conglomerate beneath may suggest, a stream-flow origin (Glennie, 1970). Alternation of these different type conglomeratic units suggests that the Aşağıçiğil

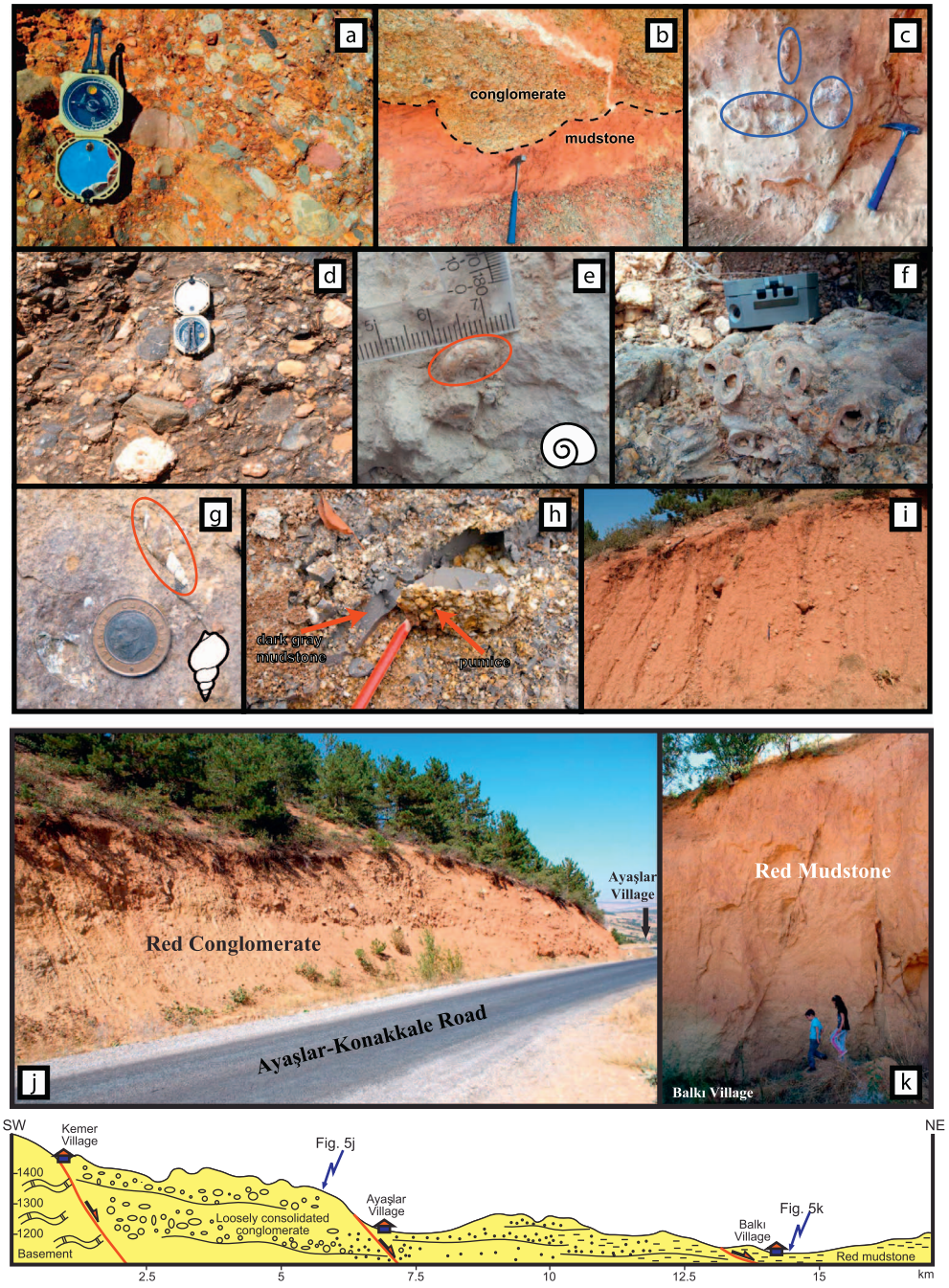

Fig. 5. (a) Close-up view of the polymict, angular to sub rounded, poorly sorted red conglomeratic unit, (b) scour-and-fill structure formed at the base of the conglomerate unit, and (c) bioturbated mudstone unit (indicated with blue circles) of the FdF. (d) Clast-supported basal conglomeratic unit, (e) fresh water gastropods bearing siltstone/mudstone and (f) fresh water stromatolitic limestone alternation of the Aşağıçiğil Formation. Measured section of the Aşağıçiğil Formation succeeded by (g) fresh water gastropods bearing mudstone, marl alternations with (h) pumice level from which sample was collected for Ar/Ar dating. (i) Conglomeratic unit of the Belekler Formation. Note that the formation characterizes loosely consolidated angular conglomerates (j) in the west of the basin and it consists of mudstone (k) in the central part of the basin. Cross-section interprets the grain size changes of the Belekler formation from margin to center of the basin. (For interpretation of the references to color in this figure legend, the reader is referred to the web version of this article.)

Formation was deposited in alluvial fan to braided to low sinuosity fluvial environment where slope and channel processes played a role. Particle size gradually decreases from western margin towards the east, which indicates facies organizations from basin margin to basin center that changes from coarse grained to mud/clay, marl, and limestone facies towards the interior part of the basin. Organic rich levels may indicate marshy areas in the periphery of a lake (Walker and James, 1992; Talbot and Allen, 1996). These lithologic characteristics and fresh water fossil content suggest a shallow lacustrine environment. Intercalation of fine grained units with conglomerates in the whole sequence indicates that the depositional environment of the Ilgın Basin laterally and vertically intercalates with alluvial-fluvial to a lacustrine environment which may involve drying out of the lake intermittently during the Middle Miocene.

3.3. Belekler Formation

The Belekler formation is characterized by reddish-brown, poorly consolidated conglomerate, sandstone, and claystone alternations. These sediments are widespread in the basin near Belekler. To the west of the Ilgın Basin, near Ayaşlar and around Balkı, topography provides a well-exposed outcrop of the Belekler Formation. The formation was first named by Umut et al., (1987) and its type locality is near Belekler (Fig. 3). The Belekler Formation unconformably rests on the Aşağıçiğil formation (Fig. 4c and b) in the southern part of the basin. A similar relationship was observed in the northern part of the basin, as well. To the SW of Ayaşlar, the formation is composed of loosely cemented, poorly sorted, pebble- to block-size (occasionally up to 50 cm diameter), matrix-supported conglomerates (Fig. 5i). Clasts generally angular, consisting of polymict limestones, quartzites and schists, i.e., lithologies that are abundant in the basement of Ilgın Basin. The clasts

Table I
Summary of $^{40}Ar/^{39}Ar$ data. Full data tables are given in the supplementary data. Errors are reported with 2σ uncertainty and represent analytical error. Full external errors are reported between brackets. MWSD is Mean Square Weighted Deviate. N is the number of analysis included in the weighted mean age, between brackets the number of experiments excluded.

Irradiation ID	Lat	Long	Meterial	Weighted Mean Age	MSWD	N	Inverse isochron	40Ar/36Ar Intercept
VU78B-S4	38.080778	31.883544	Sanidine	11.61 ± 0.05(0.24)	1.59	9(1)	11.62 ± 0.05(0.24)	286 ± 58

Errors are reported with 2σ uncertainties and represent analytical error. Full external errors are reported between brackets. MWSD is Mean Square Weighted Deviate. N is the number of analysis included in the weighted mean age, between brackets the number of experiments excluded.

are floating in a reddish muddy/sandy matrix. Conglomerates are generally structureless/massive and they do not display any primary sedimentary structures.

Towards the east, around Balkı, the facies changes laterally and the grain size gradually decreases into mudstone (Fig. 5j and k). The distal part of the sequence is composed of alternation of red mudstones and white marls. The maximum thickness of the unit was reported by Koçyiğit et al. (2000) as 319 m for the alluvial fan deposits and 280 m for the flood plain deposits based on data from boreholes provided by Çuhadar (1977). In this study, the minimum thickness of fine grained deposits representing relatively basinal facies is measured to be 200 m.

Saraç (2001) reported fossil vertebrates including *Hipparion* sp. and *Gazella* sp. from the fluvial deposits located around Belekler (Ms4 horizons in Fig. 2) and Argıthanı (Ms5 horizons in Fig. 2) town. This fossil fauna is characteristic for the MN9–12 zone so it is assigned Late Miocene age to this unit. Similarly, Koçyiğit et al. (2000) reported fossil vertebrates from lacustrine deposits in the Argıthanı (M4 horizon in Fig. 2) and Gözpınarı village (M5 horizon in Fig. 2). Samples indicate that age of this unit is Early-Middle Pliocene. This constrains the age of the Belekler formation to range from Late Miocene to Middle Pliocene.

Thick, structureless, matrix-supported conglomerates of Belekler formation, which mainly crop out at the margin of the basin. Fine-grained mudstone units with freshwater gastropods represent transitions from an fluvial to lacustrine depositional environment. Alternation of these mudstone levels with the white claystone/marl unit towards the center of the basin indicates a lacustrine paleo-environment. This indicates that the Ilgın Basin was characterized by facies associations, from the basin margin to the basin center, ranging from alluvial fan, low sinuosity fluvial to back swamps and lacustrine environment.

3.4. Quaternary

The Quaternary units in the basin are represented by alluvial deposits along permanent and temporary streams, and are found adjacent to the Çavuşcugöl Lake in marshy environments around the streams. The oldest Quaternary units are encountered close to Dursunlu village (M6 in Fig. 2). From this locality Koçyiğit et al. (2000) provided a long list of mammal fossils, including *Lepus* sp., *Ochotona* sp., *Mimomys savini*, *Lagurus arankae*, *Microtus* (Allophaiomys) *nutiensis*, *Ellobius* sp., *Apodemus* sp., *Micromys* sp., *Allactaga euphratica*, *Cricetulus migratorius*, *Mesocricetus auratus*, *Spalax leucodon*, *Spermophilus* sp., *Trogontherium cuvieri*, *Carnivora* sp., *Mammuthustrogenthherii*, *Equus* sp., *Hippopotamus trogentherii* sp., *Cricetulus* sp. and *Bos primigenius*, these fauna indicate Early Pleistocene.

4. $^{40}Ar/^{39}Ar$ geochronology

Age assignments for the Ilgın Basin so far rely on mammalian fossil fauna and spores/pollen assemblages (Koçyiğit et al., 2000; Saraç, 2001 and Karayiğit et al., 1999). To acquire absolute age data, we provide an $^{40}Ar/^{39}Ar$ age from pumice fragments found in a horizon in the Aşağıçiğil formation (Fig. 5h).

Pumice was extracted from clay layers in the Aşağıçiğil formation (see Fig. 5h and supplementary data). Bulk samples were crushed, washed and sieved. Grain size fractions of 1000–2000 μm or 500–1000 μm were used for standard magnetic and heavy liquid separations. Sanidine crystals from the pumice were separated in a final step by hand-picking under a microscope. The samples were wrapped in Al-foil packages and loaded in a 9 mm ID quartz vial. Fish Canyon Tuff sanidine (FCs) standard was used as neutron fluencemonitor. The vial was irradiated for 10 h in the OSU Triga CLICIT facility, USA. After irradiation, samples and standards were loaded in 2 mm diameter holes of a copper tray and placed in an ultra-high vacuum extraction line. Single crystal $^{40}Ar/^{39}Ar$ fusion experiments were performed at the Vrije Universiteit Amsterdam, The Netherlands using a Synrad 48–5 CO2 laser and custom made beam delivery system. Samples were purified in an in-house designed sample clean up line and analyzed on a MAP215–50 noble gas mass spectrometer equipped with a Balzers SEV217 detector. Mass discrimination was monitored by 3 replicate runs of air pipettes every 12 unknowns and blanks were run every 3 unknowns.

Ages are calculated using the in-house (Vrije University of Amsterdam) developed ArArCalc software (Koppers, 2002) with Steiger and Jäger (1977) decay constants and they are calculated relative to the FCs of 28.198 ± 0.23 Ma (Kuiper et al. 2008, note that this study reports 28.201 Ma using decay constants of Min et al., (2001) which converts to 28.198 Ma using Steiger and Jäger, 1977). Correction factors for neutron interference reactions are $(2.64 \pm 0.04) \times 10^{-4}$ for $(^{36}Ar/^{37}Ar)_{Ca}$, $(6.73 \pm 0.08) \times 10^{-4}$ for $(^{39}Ar/^{37}Ar)_{Ca}$, $(1.211 \pm 0.006) \times 10^{-2}$ for $(^{38}Ar/^{39}Ar)_{k}$ and $(8.6 \pm 1.4) \times 10^{-4}$ for $(^{40}Ar/^{39}Ar)_{k}$. The $^{40}Ar/^{36}Ar$ ratio of 295.5 of Nier (1950) is used in the calculations. Errors are reported at 2 sigma level. Outliers are identified by comparing MSWD with the T-student distributions. The summary of the $^{40}Ar/^{39}Ar$ result is given Table I and plateau and isochron is given in Fig. 6.

Sample VU78B-S4 containing high sanidine yields a weighted mean age of 11.61 ± 0.02 Ma (analytical error); or ± 0.24 Ma (full external error including standard age and decay constant uncertainties). The sample has high radiogenic $^{40}Ar^{*}$ contents and therefore data points cluster together on the isochrones.

This age is consistent with age assignments based on fossil contents.

5. Structural geology

The major structures that shaped the Ilgın Basin include large scale normal faults, numerous mesoscopic faults generally with no more than a few meters offset, and open folds and undulations. We mapped most of these structures at first using remote sensing techniques and subsequently verified their nature in the field. Kinematic data were then collected from these mesoscopic faults for reconstruction of paleostress configurations.

5.1. Remote sensing study

During the extraction of lineaments, various enhancement techniques were used to improve the spectral and spatial resolution of the used images that includes Landsat TM and ETM^{+}. In addition, Quickbird images obtained from Google Earth were used for areas where higher spatial resolution was required. Low resolution (30 m) multispectral bands of the Landsat ETM + were combined with a high resolution panchromatic image (15 m) to generate a higher resolution

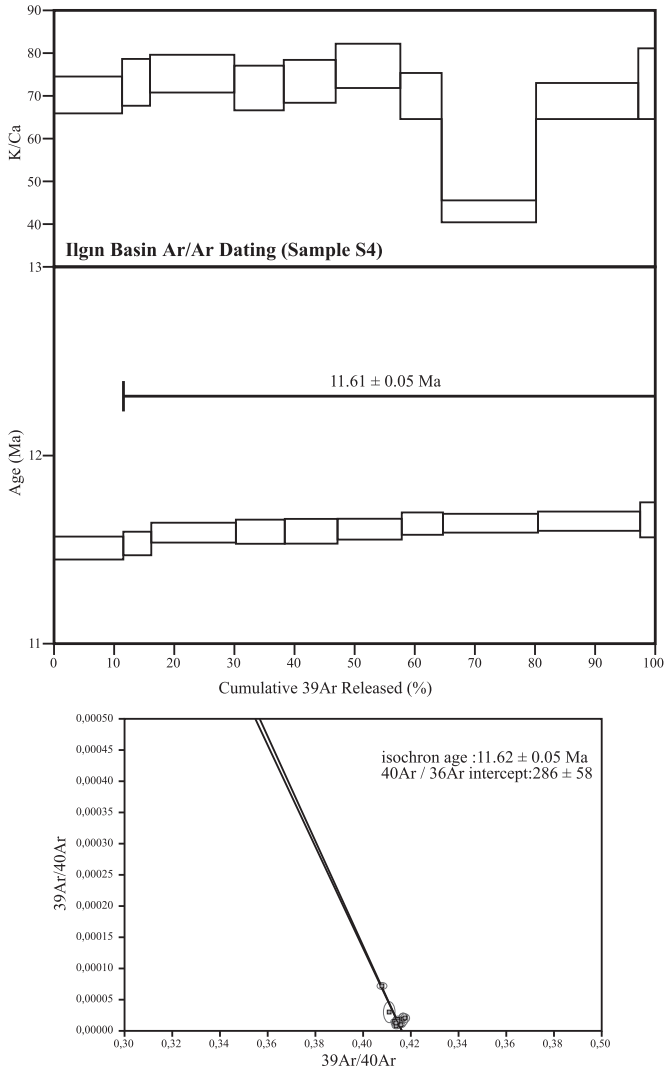

Fig. 6. Replicate single crystal fusion steps $^{40}Ar/^{39}Ar$ ages are plotted versus the % of $^{39}Ar_K$ in each fusion step relative to the combined total amount of $^{39}Ar_K$ released in all analyses for sanidine of pumice sample from the Ilgın Basin. The width of the bars/steps represents the 2σ analytical error. On top the K/Ca ratio (gray area, width is 2σ error) is displayed. Weighted mean ages are given. The lowermost graph shows the inverse isochron diagram.

fused color image (pansharpening). This process is used to improve spatial resolution of multispectral channels of the satellite images. In addition to satellite images, 25 × 25 m resolution digital elevation models (DEMs) prepared from 1/25.000 scale topographic maps were used, together with 90 × 90 m (3 arc sec) resolution Shuttle Radar Topographical Mission (SRTM) data. These images and DEMs have different spatial resolution, which is useful for detection and delineation of structures at different scales.

Digital image processing techniques including contrast enhancement, color composite, principal component analysis (PCA) and decorrelation stretching (DS) techniques, were used to enhance the spectral resolution of the images to improve the visual interpretability. All these images were co-registered using 1/25.000 scale topographic maps and combined in a GIS medium, and draped on the DEMs for 3D visualization in different directions, enhancing morphological expressions of the structures in all directions. After the images were spatially and spectrally enhanced, lineaments were delineated manually on the images. Lineaments showing appreciable morphological expressions were labeled as faults. Digital elevation data and resultant lineament map are shown in Fig. 7 together with weighted segment rose diagram prepared from the strikes of these structures. The linemanets cluster into three dominant directions (NE-SW, NW-SE and E-W). Lineaments with NE-SW orientation correspond also to well-developed river networks which is approximately at 90° angles to the NW-SE directed Akşehir Fault. E-W directed lineaments reflect secondary faults bifurcated and curved away from the major fault, here deemed the Akşehir Fault, displaying horse-tail pattern (Fig. 7).

5.2. Field observations

The major structures that bound the Ilgın Basin are normal faults. Morphologically the most prominent structure bounding the Ilgın Basin is the *Akşehir Fault Zone (AFZ)* that delimits the southwestern margin of the basin and it is very well expressed by a sharp and linear boundary between the basement and basin infill. The fault zone is > 400 km long and associated with a vertical throw of up to 2000 m between the Ilgın Basin floor and the Sultandağları high. At the western margin of the Ilgın Basin, the fault boundary is inferred mainly on the basis of a thick accumulation of red clastics originated from the Sultandağları range abutted against basement rocks. The main fault plane dips northeasterly (Fig. 7) between ~30° and 85° (see also Koçyiğit and Özacar, 2003). Morphologically, the northern continuation of the Akşehir Fault is clearly traceable on satellite images, and can easily be extracted from the DEM. The southeastern continuation is harder to discern owing to a more gradual change in elevation. Additionally, the Akşehir Fault bifurcates into several segments similar to a horsetail structure (Fig. 7). The sudden break in slope, the well-developed fault scarp, including multiple triangular facets, formation of the hanging wall valley and juxtaposition of different lithologies are considered as primary geomorphologic criteria for the recognition of the fault. Additionally, Koçyiğit and Özacar (2003) reported outcrop observations of slickensides with striations suggesting that the main fault of the fault zone – the Akşehir Master Fault - is an oblique-slip normal fault dipping at average 60 NE with a minor amount of dextral and/or sinistral strike-slip (Fig. 7). The orientations of the principal paleostresses given by Koçyiğit and Özacar, (2003) are as follows: σ1 = 241°N/76°, σ2 = 124°N/06° and σ3 = 032°N/13° and suggesting NE-SW directed extensional deformation.

The *Ilgın Fault Zone* (IFZ) is a well-exposed structure comprising a 50 km long N–S trending normal fault, with a vertical displacement of at least 240 m between basin floor and Afyon basement units. It controls the eastern margin of the Ilgın Basin and separates Miocene Ilgın Basin fill (footwall block) from the Pliocene-Holocene Çavuşçu graben (hanging wall block). An approximately N–S trending abrupt break in topography provides morphological evidence for presence of the fault. The main fault plane dips due east and the dip of the curved fault surface ranges between 45° and 88° (Fig. 7). The northern continuation of the Ilgın Fault is clearly traceable along the western boundary of the Çavuşçu Graben, then it dies out within the high topography. The Ilgın Fault preserves its N–S orientation along the Çavuşçu Lake and changes its orientation near Ilgın town center by about 20° towards a northeasterly direction after which it disappears in the vicinity of Eldeş (Fig. 3). Along the Ilgın-Çavuşçu Lake road, fault scarps are exposed. These fault scarps were developed within the metamorphic basement rocks and are coated by reddish/white fault clay. Adjacent to the fault surface, intensely fractured and brecciated rocks with variable sized angular clasts clearly identify the fault zone. In Ilgın town center, hot springs are common and some fault surfaces are altered by upwards percolations of the geothermal waters. Therefore, most of the slickensided fault surfaces are most probably washed out during this process. However, the observed slickenlines on the fault surfaces show generally down-stepping characteristics, which indicate a normal sense of displacement. Rake of the slickenlines range from 35° to 87° (Fig. 7). The shallower values of the rakes come from undulations of fault surfaces. Lower hemisphere stereographic projection of the collected fault-slip data from the IFZ is also given in Fig. 7 and it indicates *E*-W

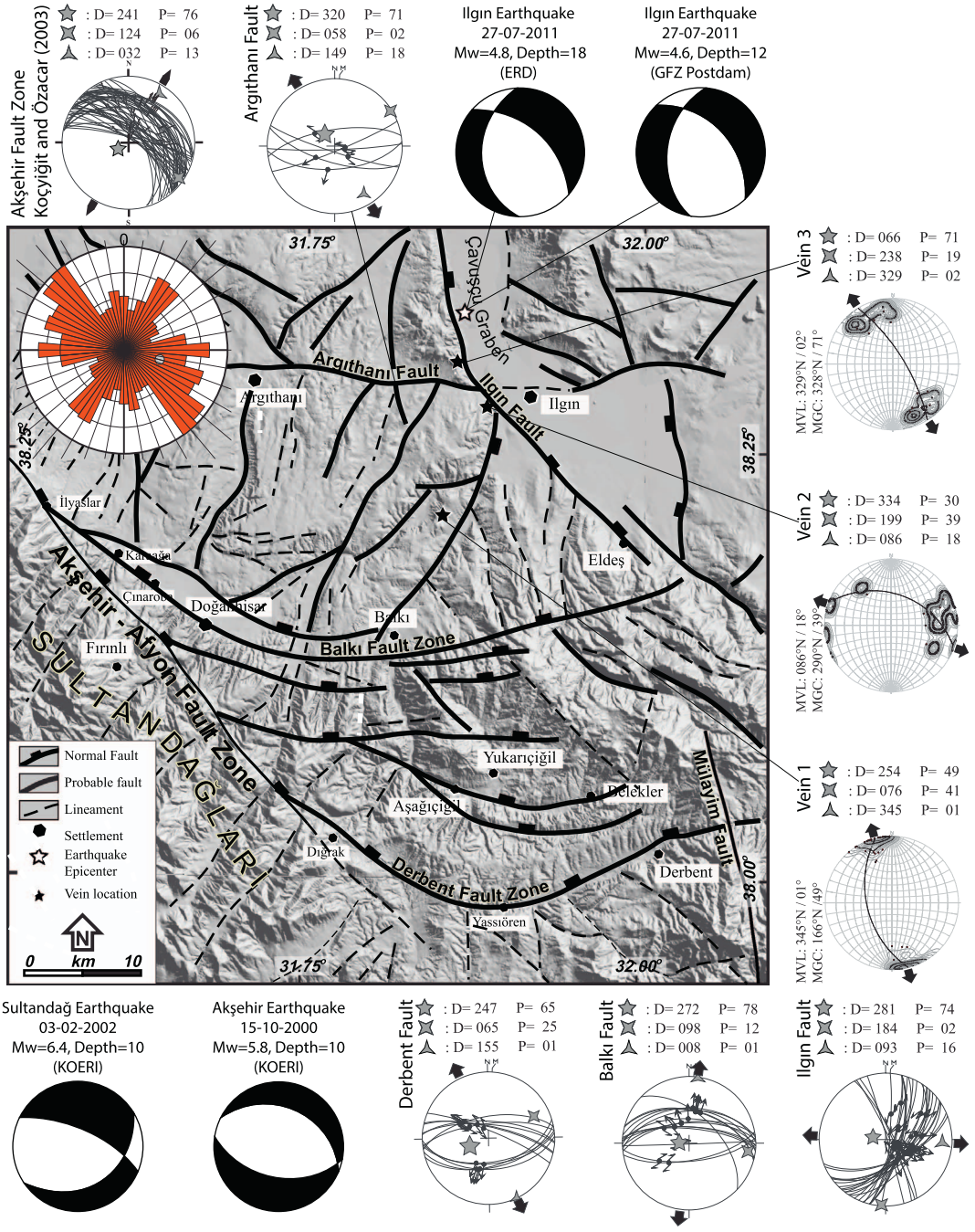

Fig. 7. Lineament map of the Ilgın Basin. Rose diagram (length weighted) shows orientations of both faults and lineaments. Base image is Digital Elevation Model produced from the 1/25.000 scale topographic maps. Focal solutions are belong to 27 July 2011 Ilgın Earthquake (M = 4.7 ERD and M = 4.6 GFZ) and 3 February 2002 Sultandağ Earthquake (M = 6.4 Taymaz et al., 2004). Paleostress solutions are given for major faults in the basin. (For interpretation of the references to color in this figure legend, the reader is referred to the web version of this article.)

directed extension. Therefore, a sudden break in slope, juxtaposition of different lithologies, formation of fault breccia (& clay), hyrothermal alteration, hot springs and well-developed slickensides are used as criteria for the recognition of the IFZ. The stereographic plot of fault-slip data shows extensional deformation and the orientation of the inferred principal stress and the stress ratio are as follows: σ1 = 281°N/74°, σ2 = 184°N/02°, σ3 = 093°N/16° (Fig. 7). The stress ratio is Φ = 0.506, and it indicates tri-axial stress condition. Well-preserved fault planes with slip lines are consistent with its ongoing activity as evident from 27 July 2011 Ilgın earthquake, (Mw = 4.8) along the fault (Fig. 7) (Hüseyinca and Eren, 2007).

In the southern part of the Ilgın Basin, *E*-W trending splay faults bifurcate from the NW-SE oriented Akşehir Fault Zone and form three major fault segments namely 1) the Argıthanı Segment, 2) the Balkı Segment and 3) the Derbent Segment (Figs. 3 and 7), together making-up the *Argıthanı-Balkı-Derbent Fault Zone* (ABDFZ). These segments are studied for the first time in detail in this study. The *Argıthanı Segment* is located in the north of the basin and is approximately 40 km long. It bifurcates from the Akşehir Fault in the vicinity of the Akşehir in the west, continues towards Argıthanı and is delimited by Ilgın Fault north of the Çavuşçu Lake in the east. The trace of the Argıthanı Segment is difficult to observe in the field and also on satellite images due to absence of any prominent topographic scarp. Koçyiğit and Özacar (2003) reported that Argıthanı Segment is north dipping normal fault without

providing any morphological nor kinematic indicators such as sudden no topographic changes, presence of fault rocks or slickensided surfaces. However, two destructive earthquakes (the 1921, September 26 Argıthanı-Akşehir earthquake (Mw = 5.4) and the 1946, February 21 Ilgın-Argıthanı earthquake (Mw = 5.5)) were located very close to this fault segment (Taymaz and Tan, 2001). Along the road between Argıthanı and Ilgın, a small fault scarp is exposed. It is oriented approximately E-W, which is compatible with the inferred trend of the Argıthanı Segment (Fig. 7). It shows very steep dip amount ranging between 75° and 90° to the south. The slickensides colected on the fault plane indicate that it is a normal fault (Fig. 7). The constructed stress configurations based on fault-slip data indicate that the orientation of the principal stresses and the stress ratio are as follows: σ_1 = 320°N/71°, σ_2 = 058°N/02°, σ3 = 149°N/18° and Φ = 0.299 (Fig. 7). These results indicate extensional deformation. Small magnitude of stress ratio indicate near uniaxial stress considitons where σ_1 is very large while σ2 and σ_3 magnitudes close to each other.

The *Balkı Segment* is the central segment of this fault zone and is approximately 45 km long. It bifurcates from the Akşehir Fault in the vicinity of İlyaslar in the west, cuts through Karaağa, Çınaroba, and then bends left around Doğanhisar towards Balkı (Fig. 7). It dies out at the vicinity of Eldeş in the east. The trace of the Balkı Segment is clearly extracted from the topographic break which shows an abrupt change in the elevation around Doğanhisar and Balkı. The Balkı Segment is encountered in the field at a small outcrop in a road cut 2 km south of the Eldeş. In this locality it juxtaposes limestone basement units and Lower to Upper Miocene lacustrine sequences of the Aşağıçiğil Formation. Fault planes of the Balkı Segment show well-developed slickensided surfaces with well-preserved slickenlines. Fault planes dip towards the north at angles of 46° to 89° and rakes of slickenlines range between 52° and 88° (Fig. 7). The hanging wall block is located to the north of the fault zone. The stereographic plot of slip data collected from indicate that the orientation of the principal stresses and the stress ratio are σ1 = 272°N/78°, σ2 = 098°N/12°, σ3 = 008°N/01° (Fig. 7) and Φ = 0.391 again illustrating extensional deformation.

The *Derbent Segment* is the southernmost major splay fault bifurcating from the Akşehir Master Fault and is located at the southern edge of the basin. It is approximately 40 km long and splays from the Akşehir Fault to the north of Dığrak. From Dığrak to Yassıören, it has an approximately NW-SE trending trace, and then bends to the left and then strikes *E*-W from Yassıören to Derbent and further east along a river channel in Ilgın Basin to the Altınapa Basin. These two river channels are separated from each other by the Mülayim Fault (Koç et al. 2012) (Fig. 7). Morphologically, an approximately E-W trending north dipping fault scarp is easily recognized in the field by the abrupt change in topography towards the northern downthrown block. The fault plane of the Derbent Segment is covered by an apron of alluvial fan deposits possibly due to high sedimentation rates with respect to the fault displacement rate. Therefore, fault-slip measurements could be obtained only from short fault segments that are developed parallel to the Derbent Segment. In an outcrop along the Ilgın-Derbent road at 4 km north of Yassıören, the cross-sectional view of a lacustrine limestone unit belonging to Aşağıçiğil formation is displaced by Derbent segment. The fault plane shows well-developed slickenlines which indicate normal sense of movement (Fig. 7). In this locality the fault zone also has conjugate sets. On these faults, fault-slip data were collected and the measurements indicate fault planes dips towards both north and south with angles of 46° to 89° and rakes of slickenlines range between 50° and 82° (Fig. 7). The constructed paleostress configurations are consistent with the normal character of the fault. The orientation of the principal stresses and the stress ratio are σ1 = 247°N/65°, σ2 = 065°N/25°, σ3 = 155°N/01° and Φ = 0.126 (Fig. 7) and vertical major principal stresses confirm extensional deformation while small stress ratio indicate uniaxial stress conditions.

6. Paleostress analysis of mesoscopic faults

6.1. Data and methods

In addition to the large-scale structural analysis, we carried out detailed kinematic analyses from mesoscopic structures to unravel paleostress configurations during the development of the Ilgın Basin. For this purpose, we used Angelier's direct inversion routine (INVD) (Angelier, 1994) on fault slip data.

Analysis of fault attitude and their associated directions and sense of motion are used to infer principal stresses (Angelier, 1990, 1994; Carey and Burinier, 1974, Etchecopar et al., 1981). The result of the analysis contains information of the stress condition that were responsible for brittle deformation events. During this analysis, four assumptions are fundamental: (1) the bulk state of stress in a small area is uniform, (2) the slip direction is parallel to the maximum resolved shear stress on each faults (Wallace, 1951-Bott, 1959 assumption), (3) all movements occur under a same stress tensor and (4) the strain is non-rotational. Paleostress analyses determine the best fitting reduced stress tensor based on the collected fault slip data, identifying the orientations of three principal stresses (σ_1: maximum, σ_2: intermediate, σ_3: minumum) and the shape ratio of stress ellipsoid, $\Phi = (\sigma_2 - \sigma_3) / (\sigma_1 - \sigma_3)$ ranging between two extreme values of 0 and 1. The Φ ratio constraints allpossible cases between uniaxial ($\sigma_2 = \sigma_3$; Φ = 0 or $\sigma_1 = \sigma_2$; Φ = 1, uniaxial) and tri-axial stress configurations ($\sigma_1 > \sigma_2 > \sigma_3$; Φ = 0.5).

Another data set used to construct and to analyse paleostress configurations concern veins. Dunne and Hancock (1994) argued that mineral growth directions are perpendicular to fracture walls (Mode-I fractures) and are parelell to σ_3; therefore, it provides minor principal paleostress orientations. The vein poles corresponds to the minimum effective principal stress (σ_3). However, they do not provide precise constraints on the orientation of intermediate and major stress directions.

6.2. Fault-slip analysis

A total of 561 fault-slip measurements including orientations of the fault planes, slip directions and sense of relative movements were collected from 47 locations of mesoscopic faults cutting Ilgın Basin infill, as well as from the major fault zones (see supplementary data and Table II). Rose diagram of strikes of these fault planes indicates dominant E-W and NE-SW orientation. Dips of the faults range from 30° to 90°, with the majority between 50° and 75° (see supplementary data).

51 stress configurations from 47 locations were constructed (see supplementary data and Table II). During the analysis, Maximum Angular Deviation (ANG) and Quality Estimator (RUP) values were chosen as 22.5° and 45°, respectively. The smaller values are regarded as a good match (Angelier, 1994). Faults with greater angular deviations were considered as spurious and they were not used in the construction of the stress tensor. In this data set, 32 fault slip measurements are regarded as spurious, which is approximately 5.7% of the whole data set.

Using the misfit criteria and separation procedure, sites 11, 17, 38 and 40 produced two different paleostress configurations even though they were collected from same unit and the same locality. This situation may refer to heterogeneity of fault slip data (Angelier, 1979; Armijo et al., 1982; Huang and Angelier, 1989; Yamaji, 2000) caused by polyphase or non-coaxial deformation. For those, each slip direction was analyzed separately and separated configurations are labeled as 'B' in Table II.

Syn-sedimentary faults are crucial for paleostress stratigraphy, since the age of the faults can be determined from the age of the sedimentation. In site 13 and 34, step-like *syn*-sedimentary faults with dip-slip movement were found in the higher levels of the Kumdöken formation. The strike of the measured faults is approximately E-W and inferred extension direction from these locations is N(W)-S(E). Similar

Table II
Table showing all paleomagnetic data from this study.

Loc	Long	Lat	σ_1(D°/P°)	σ_2(D°/P°)	σ_3(D°/P°)	Φ	Mean ANG	Mean RUP	N
I1	31.85088	38.19095	040/83	260/05	169/04	0.445	9	29	11
I2	38.12399	31.66351	130/62	291/27	025/08	0.087	13	44	10
I3	38.11452	31.73580	090/61	291/27	197/09	0.114	14	34	7
I4	38.11331	31.73529	043/85	305/01	215/05	0.215	9	26	16
I5	38.12139	31.81230	021/69	258/12	165/17	0.232	14	34	7
I6	38.01675	31.89772	065/63	258/26	165/05	0.840	18	36	12
I7	38.02812	32.02481	294/65	115/25	025/00	0.383	17	39	10
I8	38.31920	31.85933	211/71	358/16	091/10	0.074	13	43	11
I9	38.29280	31.75265	248/71	345/03	076/19	0.392	12	37	12
I10	38.34614	31.85381	330/81	087/04	177/08	0.206	16	51	10
I11A	38.34614	31.85381	342/70	171/20	080/03	0.449	11	23	30
I11B	38.29517	31.75802	281/74	184/02	093/16	0.506	16	36	29
I12	38.08479	31.82328	086/83	340/02	250/07	0.514	6	14	14
I13	38.08488	31.82334	330/74	060/00	150/16	0.374	12	29	6
I14	38.01720	31.89772	272/14	120/74	004/07	0.661	7	13	7
I15	38.01865	31.89784	247/65	065/25	155/01	0.126	7	30	12
I16	38.08604	31.82481	290/82	133/08	042/03	0.182	10	35	18
I17A	38.08604	31.82481	085/83	294/06	204/03	0.324	4	9	6
I17B	38.11204	31.73563	190/61	351/27	085/08	0.739	2	5	6
I18	38.11204	31.73563	241/78	098/10	007/07	0.431	12	26	14
I19	38.18345	31.99435	295/65	089/23	183/10	0.166	20	38	13
I20	38.18974	31.99170	301/74	078/12	171/10	0.141	6	14	4
I21	38.11608	31.82401	011/76	245/08	153/11	0.153	5	11	9
I22	38.11741	31.82146	008/68	239/14	145/16	0.218	4	26	9
I23	38.10466	31.79358	005/72	104/03	195/18	0.380	14	36	17
I24	38.05904	31.81691	287/71	017/00	107/19	0.460	6	28	8
I25	38.17599	31.83689	275/74	056/13	148/10	0.418	19	57	11
I26	38.14568	31.75565	020/70	287/01	196/20	0.372	2	24	5
I27	38.07674	31.84462	043/71	299/05	207/18	0.376	13	34	15
I28	38.07667	31.84400	087/56	287/33	191/06	0.770	11	22	17
I29	38.07489	31.84275	333/60	178/28	082/11	0.218	6	18	7
I30	38.05650	31.81689	046/76	252/13	160/06	0.546	16	30	5
I31	38.07508	31.82947	176/75	310/10	042/11	0.167	4	11	5
I32*	38.19082	31.85090	065/52	197/28	301/24	0.543	8	38	5
I33	38.08567	31.82396	269/13	117/76	001/06	0.313	5	10	8
I34	38.08488	31.82348	043/71	274/12	181/14	0.647	10	23	10
I35	38.08466	31.82331	276/33	060/52	174/18	0.764	6	16	14
I36	38.08432	31.82447	353/83	240/03	150/07	0.747	3	25	5
I37	38.05122	31.83894	088/52	285/36	189/08	0.622	4	15	4
I38A	38.38145	31.84358	023/65	193/24	284/04	0.155	16	31	9
I38B	38.38240	31.84318	176/68	024/20	291/10	0.262	15	38	5
139	38.38240	31.84318	059/77	202/11	294/08	0.331	7	15	8
I40A	38.38280	31.84502	167/72	267/03	358/18	0.350	10	33	8
I40B	38.32201	31.85929	341/15	231/52	081/34	0.720	11	43	7
I41	38.32201	31.85929	208/68	324/10	057/20	0.249	5	24	6
I42	38.13818	31.66580	021/89	234/01	144/01	0.363	13	26	15
I43	38.22934	31.54675	296/64	134/24	041/07	0.518	12	39	12
I44	38.38161	31.84562	060/72	209/16	301/09	0.184	4	18	6
I45	38.08150	31.84820	264/79	112/10	021/05	0.390	11	31	8
I46	38.28209	31.71155	004/62	195/28	103/05	0.174	12	26	12
I47	38.07689	31.83691	310/67	092/18	186/13	0.702	9	22	16

σ1, σ2, σ3 magnitude ratios of principle stresses; D/P, direction/plunge; Φ stress ratio; ANG, maximum allowed angular divergence RUP, maximum allowed quality value N, number of measurement for each site.

relationships were also observed within the Aşağıçiğil formation. The principal stress orientations reconstructed from the syn-sedimentary faults documented in sites 24, 29 and 36 indicate that the tectonic regime was extensional during the deposition of the Aşağıçiğil formation, Derbent Segment illustrated by vertical maximum principal stress. However two different dominant extension directions, E-W and ~N (W)-S(E) prevailed during the deposition of the Aşağıçiğil formation. Additionally, mesoscale conjugate faults are also recorded (i.e. sites 1, 2, 15, 16, 17A, 18, 19) in Pre-Neogene basement limestone and basin infill. Conjugate sets whose orientation and slip direction are also related to the principle stress axes provide a convenient way to determine reliable paleostress axes (Huang and Angelier, 1989).

During collection of the fault-slip data, NE-SW striking strike-slip faults (i.e sites 14, 33, 35) are encountered in the study area (see supplementary data). In these sites, resolved intermediate principle stress orientation were found to be vertical, which indicates transcurrent deformation. However, these data sets need not to be interpreted as separate tectonic phases since their configurations are consistent with overall N–S extension and are regarded as transfer faults between normal faults.

6.3. Veins

Veins have encountered within the Aşağıçiğil formation and in basement limestone units. Three vein sets were recognized: (1) an roughly E-W striking vein set located 2 km northwest of Göstere within the Aşağıçiğil formation, (2) dominantly NE-SW striking set located 6 km NW of the Ilgın, along the Çavuşçugöl road and (3) a rougly N–S striking set located at the western edge of the Ilgın town center within the basement limestone unit.

The first data set consists of 37 vein measurements (Vein 1 in Fig. 7). The strike of the veins ranges between 50° and 90° and their

thicknesses range from < 2 mm to up to 5 cm. Veins have one single growth band, the central part of the veins are generally still open, and blocky calcite crystals are perpendicular to the vein walls and are developed symmetrically from both walls towards the vein center, indicating pure open mode fracture,with syntaxial growth and the minor principal stress σ_3 was perpendicular to the vein wall (Dunne and Hancock, 1994). The highest frequencu of the vein poles corresponds to σ_3 which is oriented σ_3: 345°N /01, indicating the extension direction was approximately N−S during the developemnt of these veins.

The second vein data set consists of 10 vein measurements (Vein 2 in Fig. 7) and their thicknesses vary from 5 cm up to about 60–70 cm. Veins show banded structures with different color (ranging from red to dark gray) developed from walls towards the vein center (syntaxial growth). Mineral growth directions are perpendicular to the fracture wall, which shows that direction of the dilatational stress did not change during the vein formation and the minor stress was oriented σ_3: 086°N/18°, which indicates that the extension direction was approximately *E*-W during the developemnt of these veins.

The third data set contains 11 vein measurements (Vein 3 in Fig. 7) and they are about 3–4 cm thick. Growth patterns of the vein bands are symmetrical on either side of the wall rock. The crystal faces of the vein fill is not well developed, and also the comb structure is slightly observable. The strike of the veins range between 38°N and 87°N (Fig. 7). Direction of the minimum principal stress (σ_3) is 329°N/02°, which indicates that the extension direction was about NW-SE.

7. Discussion

7.1. Spatial characteristics

Paleostress analyses from the Ilgın Basin unravel the stress regimes that controlled the geometry and evolution of the basin. To this end, we performed detailed analyses of the constructed paleostress configurations and compared them with the regional structures in order to check their consistency. Fig. 8 shows the density diagram of the principal stress orientation (σ_1, σ_2 and σ_3, respectively) as well as histograms of the Φ values for the whole data set. The σ_1 direction is generally oriented (sub-)vertical in all sites except for sites (14, 33, 35 and 40B, which sites produced strike-slip solutions) as they are concentrated in the center of the diagram. Whereas the orientations of σ_2 and σ_3 directions vary but are consistently sub-horizontal. Such distributions are characteristics for uniaxial stress conditions and result in stress permutations in regions where the magnitudes of the σ_2 and σ_3 are very close to or equal to each other. The deformation that affected the Ilgın Basin is clearly extensional, as indicated by the vertical σ_1, and consistent with normal fault activity along the major faults in the basin. The nearly equal σ_2 and σ_3 magnitudes should produce Φ values approaching zero in the case of σ_1 magnitudes much greater than that of σ_2. As illustrated in Fig. 8 and Table II, the frequency distribution of Φ values has peak at 0.35 ($0.25 < \Phi < 0.75$, pure extensional). Nineteen of the Φ values is between $0 < \Phi < 0.25$ (uniaxial extensional) and 28 of Φ values are lying between $0.25 < \Phi < 0.75$ (pure extensional, well-developed tri-axial stress), which means that stress conditions may change spatially and temporally from uniaxial radial extension to triaxial well constrained and directed extension states.

To verify the compatibility of the constructed paleostress configuration relative to regional structures, the horizontal components of the σ_3 directions are plotted on the map in Fig. 9. Our field studies reveal that NE-SW and roughly E-W trending major fault sets controlled the development of the Ilgin Basin. Most of σ_3 directions, including strike-slip solutions (14, 33, 35 and 40B), also indicate two dominant extension directions. These directions seems to be related to local stress conditions rather than the regional stress pattern since the orientations of all σ_3 are almost perpendicular to the adjacent major faults. This pattern implies unconstrained slip (somewhat similar to free fall of hanging wall, as expected in uniaxial stress conditions). The sites with strike-slip solutions are related to transfer faults and/or stress perturbations due to accommodation of local space problems.

7.2. Temporal characteristics

In addition to spatial distributions, temporal changes of the paleostress configurations are crucial to unravel paleostress stratigraphy of the basin. Since some of the mezoscopic structures are *syn*-depositional structures, therefore, they recorded paleostress orientations during and after the sedimentation, while the basement likely recorded the entire paleostress evolution. Temporal characteristics of the basin are given in Fig. 10. Relative ages of the paleostress data are ordered based on (1) the age of the rocks from which the fault-slip data were collected and (2) crosscutting and overprinting relationships between the faults and the stratigraphy. The paleostress directions for all lithological formations were plotted separately (Fig. 10).

The youngest, still active extension direction in the Ilgın Basin is reflected by Afyon-Akşehir Fault zone (sites 2, 4 and 41) and Ilgın Fault Zone (sites 9, 11, 38B and 40B). These extension directions trend approximately E-W to NE-SW. This youngest tectonic regime is consistent with focal mechanism solutions of the Ilgın Earthquake (27 July 2011, M = 4.7), the Sultandağ Earthquake (3 Feb 2002, M = 6.4) and the Akşehir Earthquake (15 Oct 2000, M = 5.8). The results reveal that there is co-axial defromation since the Miocene, and two dominant E–W (~NE-SW) and ~N–S (~NW-SE) extension directions consequently acted in tandem throughout the evolution of the Ilgın Basin and still do today. From these results, we infer that present-day stress configuration migth have been prevailed since the Middle Miocene.

7.3. Fault architecture

Our structural geological results from the Ilgın Basin, combined with those from the Yalvaç and Altınapa basin (Koç et al., 2012, 2016a) now allow to develop an overview of the complex interplay between normal faults in different orientations (Fig. 11). Throughout the Central Tauride Intramontane Basin region, we found evidence in small-scale faulting for multi-directional although mainly E-W and N-S extension. When we connect all the major faults, the mozaic of Fig. 11 appears. The main basin-bounding structures (Akşehir Fault Zones and Ilgın Fault see Figs. 3 and 11) are determined by ~N(W)–S(E) striking normal faults in response to (N)E–(S)W stretching, but subordinate, yet prominent ~E–W trending (Argıthanı, Balkı Derbent Fault Zones, see Fig. 3), dip-slip normal faults accommodating ~N–S extension have continuously played a role as well. The major normal faults die out along-strike, causing complex relay ramp geometries, e.g. between the Akşehir Fault and the Ilgın Fault causing the southward decrease in elevation of the Akşehir fault and its submergence below the Beyşehir basins and Erenlerdağ volcanics. Within this mozaic of normal faults, the Yalvaç, Ilgın, and Altınapa basins formed local depocenters. These have been uplifted and incised since the Pliocene and deposition is currently ongoing in the Beyşehir and Akşehir basins (Fig. 11) due to shifting of the locus of extension. The overall extension directions remained similar from the Early Miocene to the present.

7.4. Paleogeography of the Central Taurides

Our constraints on the age and paleo-environmental setting of the Ilgın Basin, together with those of the Yalvaç and Altınapa Basins (Fig. 12) (Koç et al., 2012 and 2016), as well as the Neogene basins on top of and west of the Central Tauride mountain range allow to develop Miocene paleogeographic maps (Fig. 13). These illustrate how latest Miocene to Recent uplift of the Central Anatolian plateau must have been involved in the development of relief along the southern margin of the plateau.

The Central Tauride intramontane basins unconformably cover ophiolites, Afyon zone rocks, as well as deeper structural units of the

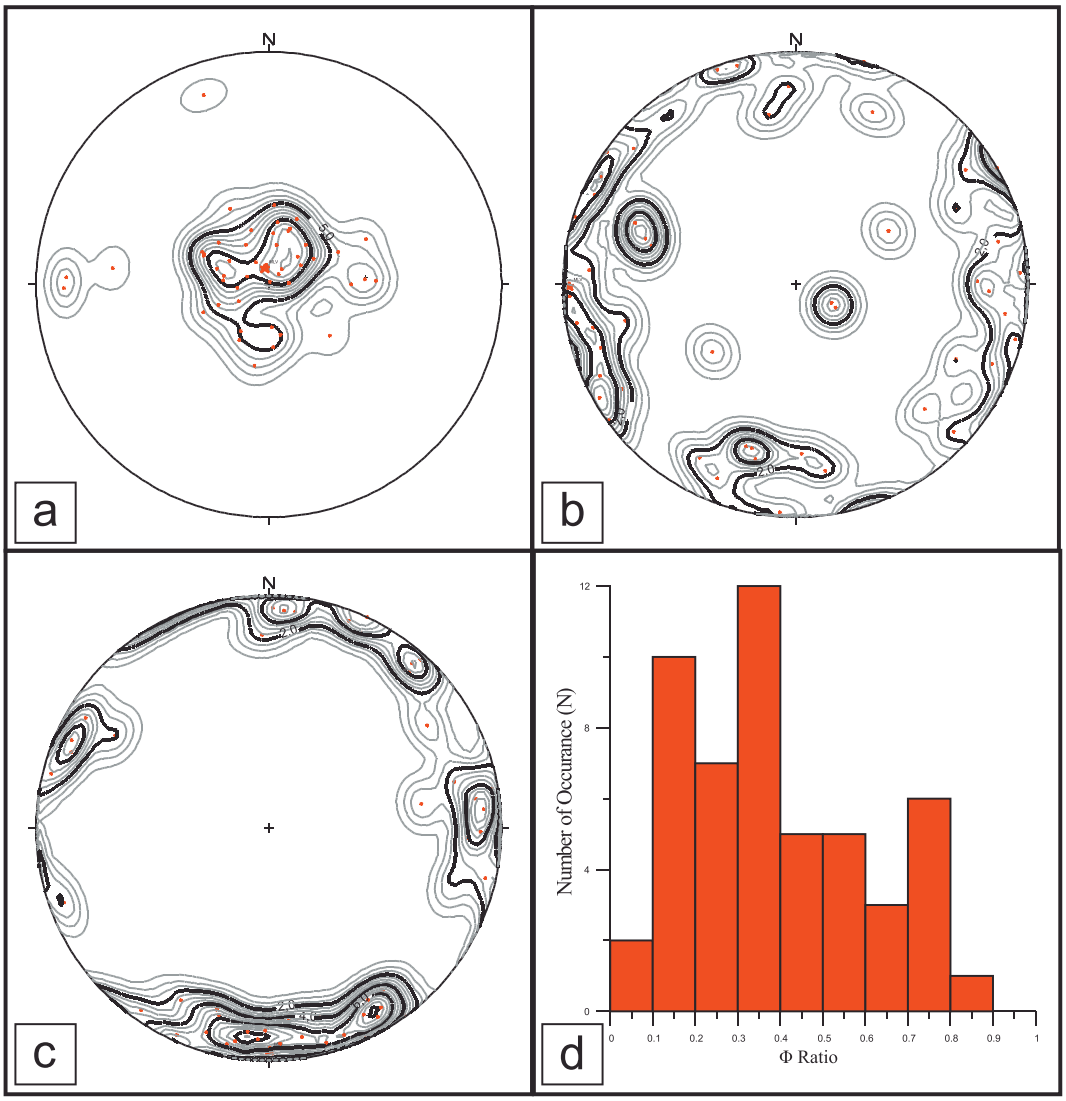

Fig. 8. Density diagrams for principle stress orientations (σ_1, σ_2 and σ_3, in a, b and c respectively) and frequency distribution of Φ values for whole data (d). Notice that the σ1 is significantly (sub-)vertical while σ2 and σ3 orientations are horizontal.

Taurides. The sedimentation in these continental basins commenced during the Early Miocene in Ilgın Basin and Middle Miocene in Yalvaç and Altınapa basins and they were likely governed by extension. The Erenlerdağ volcanic complex to the southwest of the Altınapa basin is also of Middle Miocene to Pliocene age (Besang et al., 1977, Keller et al., 1977, Temel et al., 1998; Tatar et al., 2002; Koç et al. (2012) reported a similar $^{40}Ar/^{39}Ar$ age from a lava and a pumice horizon in the Upper Altınapa Group in Altınapa Basin to the south. There is no evidence that this volcano developed in a marine basin. Hence, throughout the Neogene, the modern Central Taurides Intramontane Basin system formed a series of depocenters with lakes in the center surrounded by fluvial sedimentation systems seperated by basement highs, often bounded by normal faults. Volcanoes are found near Afyon, Sille, and Erenlerdağ (Fig. 13). Towards the south, the Ermenek subbasin in the northwestern part of the Mut basin, was dominated by continental sedimentation in Late Oligocene to Early Miocene time (Ilgar and Nemec, 2005; Esirtgen, 2014). Similar to the Central Tauride Intramontane basins, the Ermenek basin formed also as intra-montane NW-SE trending graben (Ilgar and Nemec, 2005) Continental sedimentation in the Ermenek Basin started during Late Oligocene time and lacustrine sedimentation was terminated by a late Burdigalian marine invasion (Ilgar and Nemec, 2005) (Fig. 13b).

This Burdigalian marine invasion led to widespread sedimentation in the Aksu, Köprüçay, Manavgat, and Mut basins. This allows us to estimate a zone where the Miocene paleo-shoreline must have been located in the region that is now elevated (Fig. 13a) on the eastern part of the present-day high Tauride axis, which today lies ~500–1000 m higher than the contemporaneous intramontane basins to the north and east. This shows that major differential uplift must have occurred during the Middle/Late Miocene (Koç et al., 2012). Our documented normal fault pattern likely played a prominent role in the accentuation of relief.

The potential causes of uplift of the Taurides is a hotly debated topic in Anatolian geology. Popular views invoke regional plateau rise as a result of dynamic topographic responses to slab break-off or slab segmentation below the Taurides (e.g., Schildgen et al., 2014) or mantle delamination (e.g., Bartol and Govers, 2014). Others have pointed at possible effects of southeastward emplacement of the Lycian nappe stack over Bey Dağları in the Early-Middle Miocene, to the west of our study area. (Ten Veen et al., 2009). Our results show that formation of differential relief must at least in part be caused by the extension that led to the formation of the Central Tauride Intramontane basins. Previous paleomagnetic studies showed that the Beydağları platform underwent ~20–30° post-Early Miocene CCW rotation (Kissel and Poisson, 1987; Kissel and Laj, 1988; Morris and Robertson, 1993; van Hinsbergen et al., 2010a). Koç et al. (2016a, b) showed that this

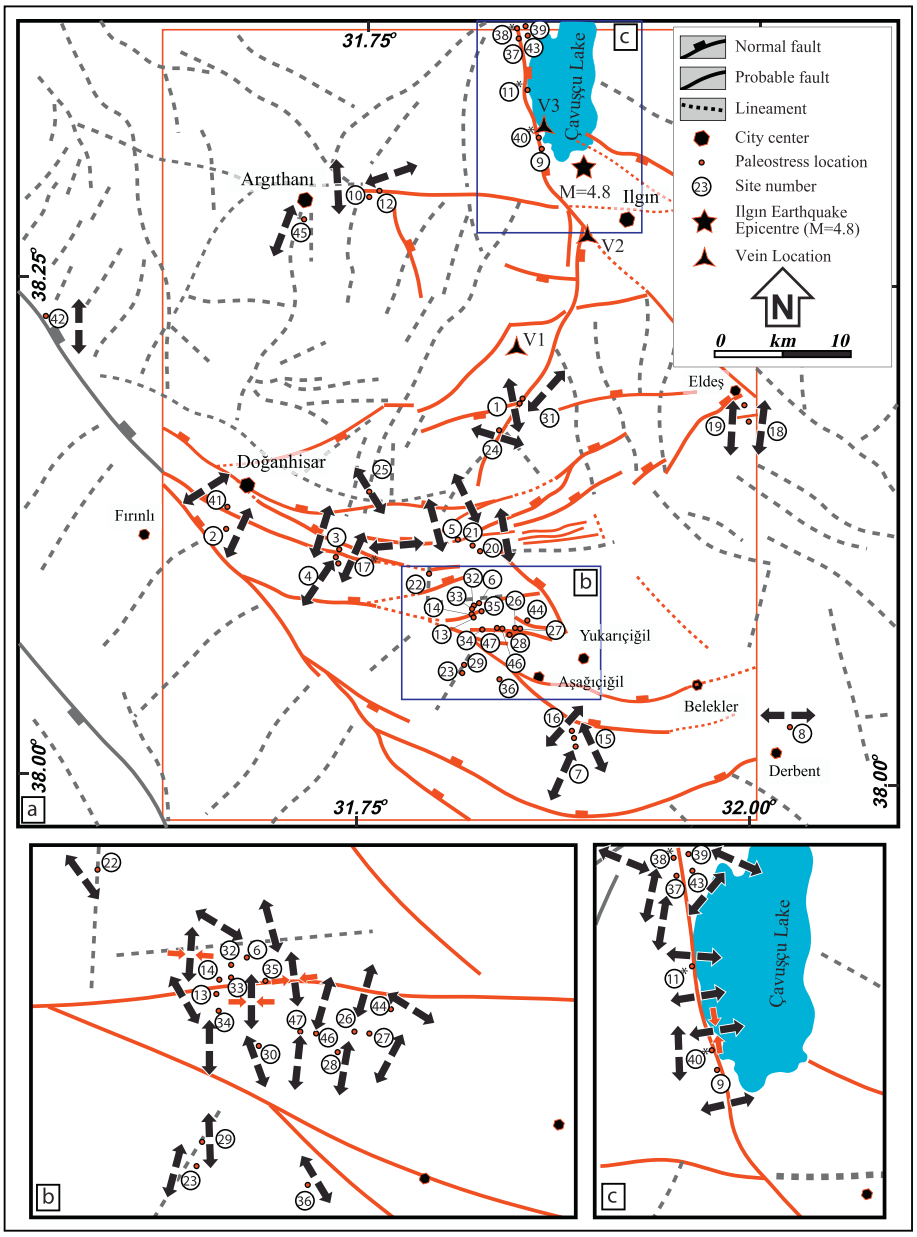

Fig. 9. Spatial distribution of the paleostress measurements on the major faults (red color) and lineament map (gray color) of the Ilgın Basin. Numbers indicate locations of paleostress and arrows indicate horizontal component of the minor principle stress (σ_3). Blue rectangle areas in the base map show the location of the close–up view of the inset maps which are labeled as b and c. Red rectangle area represents mapped area given in Fig. 3. (For interpretation of the references to color in this figure legend, the reader is referred to the web version of this article.)

rotation was accommodated by a series of thrust faults between Bey Dağları and the Köprüçay basin and argued that this shortening was balanced by the extension in the Central Tauride Intramontane Basins. To explain the shortening-extension coupling, Koç et al. (2016a, b) suggested that the tomographically imaged Antalya Slab (Biryol et al. 2011; van der Meer et al., 2017) may still have been connected to the Bey Dağları platform in the Miocene time, and its westward retreat relative to Central Anatolia drove shortening in the Isparta Angle and extension in the Central Tauride Intramontane Basins. Whilst it is certainly possible that uplift of the Central Anatolian Plateau is somehow influenced by mantle processes, such processes involve either postulated break-up, break-off, or delamination of the Antalya slab. Based on the structural data from our field area and on the paleogeographic maps we inferred from the regionally described Neogene deposits and their paleoenvironment, we suggest that much of the topography that characterizes the Central Taurides today is influenced by crustal deformation rather than mantle processes. This crustal deformation may best be explained by invoking a key role for motions of the Antalya slab relative to Central Anatolia. In any case, when studying the causes of Central Anatolian Plateau rise, the direct deformational effects of the Antalya slab on Central Anatolian geology should not be ignored.

8. Conclusion

We study the stratigraphic, sedimentological, and structural evolution of the Central Taurides Intramontane Basins and their implications for the Neogene paleogeography and tectonic history of the Central Anatolian Plateau. To this end, we provide new data on the Early Miocene and younger Ilgın Basin, located at the eastern limb of the Isparta Angle. The Ilgın Basin unconformably rests on top of pre-Neogene deformed and metamorphosed Tauride basement. A fining-upwards succession of basal conglomerates into the Lower Miocene Kumdöken Formations with fine lacustrine limestones, and clays in the center of the basin illustrate that accommodation space started to form during Early Miocene. Marginal clastic deposits of the Kumdöken Formation was unconformably covered by Aşağıçiğil Formation consisting of fine lacustrine limestones and clays indicates that the basin reached the maximum extend during Middle Miocene time (including

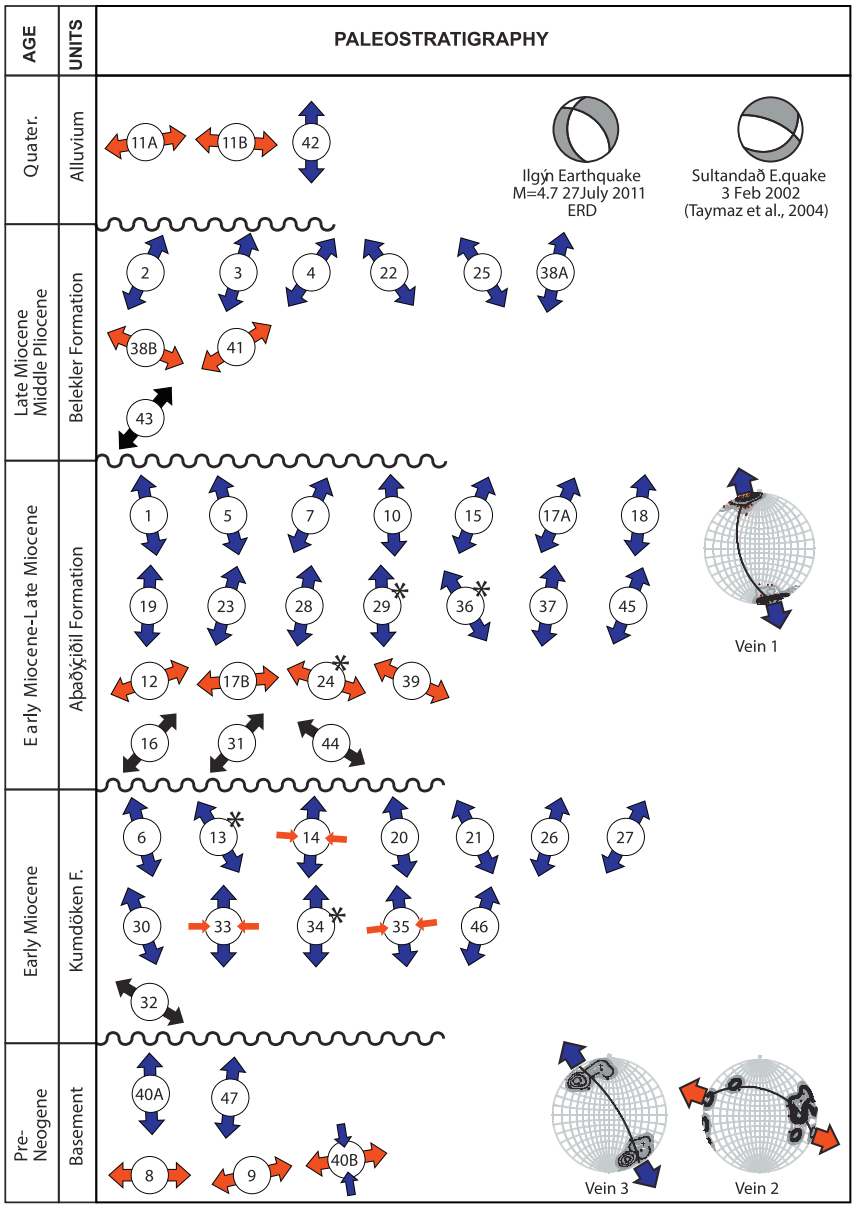

Fig. 10. Paleostress stratigraphy of the Ilgın Basin from the Early Miocene to Recent. Arrows represent σ3 directions. Red, blue and black arrows indicate *E*-W extension, N–S extension and hybrid paleostress solution, respectively. Black star are used to represent *syn*-sedimentary fault-slip solution. Focal solutions are belong to 27 July 2011 Ilgın Earthquake (M = 4.7 ERD and M = 4.6 GFZ) and 3 February 2002 Sultandağ Earthquake (M = 6.4 Taymaz et al., 2004). Stratigraphic location of the vein data is also given. Note that nature of σ3 directions and extension directions of the earthquakes and the vein data in the region. (For interpretation of the references to color in this figure legend, the reader is referred to the web version of this article.)

newly $^{40}Ar/^{39}Ar$ dated 11.61 Ma pumice fragments) and represented a local depocenter.

Our results demonstrate that the Ilgın Basin is an extensional basin and extension related subsidence was controlled along large NW-SE trending Akşehir-Afyon basin bounding fault in the west that produced half-graben geometry of the Ilgın Basin. Although the dominant extension was N*E*-SW to E-W, subordinate E-W striking normal faults are shown to have been simultaneously active throughout the history of the basin. We confim this conclusion by extensive paleostress analysis using outcrop-scale growth faults and vein sets in the basin stratigraphy. A similar history was recently documented from Yalvaç and Altınapa Basins (Koç et al., 2012 and 2016). This multi-directional remains active today as shown by seismic activity.

We use our results to develop the first integrated structural map of the Central Tauride Intramontane basins, which comprises a series of N (W)-S(E) and E-W trending major normal faults that laterally die out and connect to adjacent faults through relay ramps. This created local depocenters including the Yalvac, Altınapa, and Ilgın Basins.

We used our results complemented with constraints on marine basins in the south and west to develop first-order paleogeographic maps for the Miocene of the Central Anatolian Plateau. During the Early Miocene, the paleo-shoreline was located north of Acıpayam in the west while lacustrine Ermenek and Ilgın Basins were east of the shoreline. Following a Burdigalian marine transgression, the shoreline briefly advanced towards more internal regions in Anatolia. During this time interval, the Yalvaç Basin started to develop while the Altınapa and Ilgın basins reached their maximum extend after a major intra-Mid Miocene unconformity and are accompanied with volcanism towards the end of Serravallian. Marine continental transition in the central part of the Isparta Angle was very close to the Yalvaç Basin, especially during the Late Miocene, in which continental settings prevailed and their southern limits defined the northern edge of the marine environments. Combinations of all these information obtained both from literature and acquired in this study have very important implications for the geological evolution of southern Anatolia as well as its topography.

Our first-order paleogeographic maps and structural information show that much of the topographic relief in the Central Taurides relates to crustal deformation rather than mantle-driven dynamic topography. We concur with previous inferences that the tomographically imaged

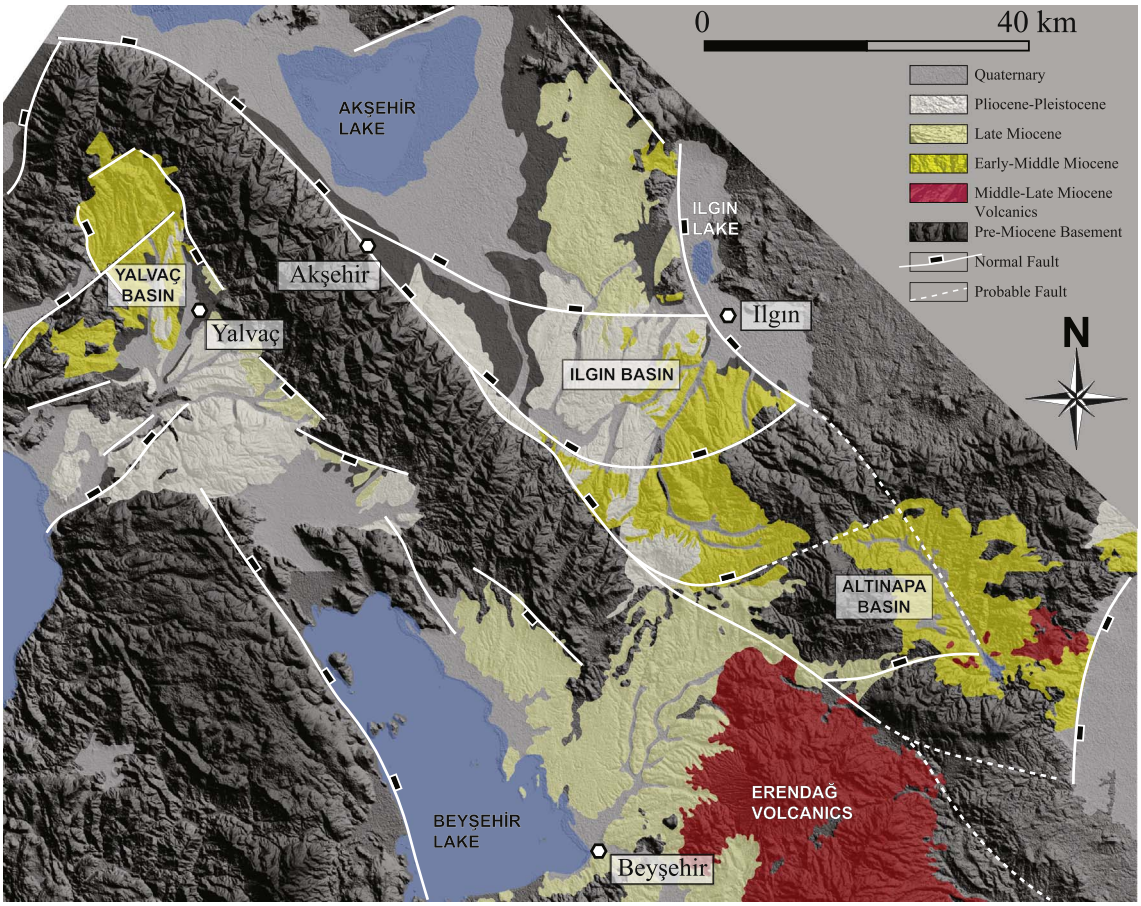

Fig. 11. Fault architecture of the region which shows a series of N(W)-S(E) and E-W trending major normal faults that laterally die out and connect to adjacent faults through relay ramps.

Antalya slab may have played a central role in causing Miocene shortening in the heart of the Isparta Angle while at the same time driving extension in the Central Tauride Intramontane Basins. The dynamic topographic effects invoked for Central Anatolia all point to break-off, break-up, or delamination caused by this slab, and we here stress that also the direct deformational effects that the motion of the

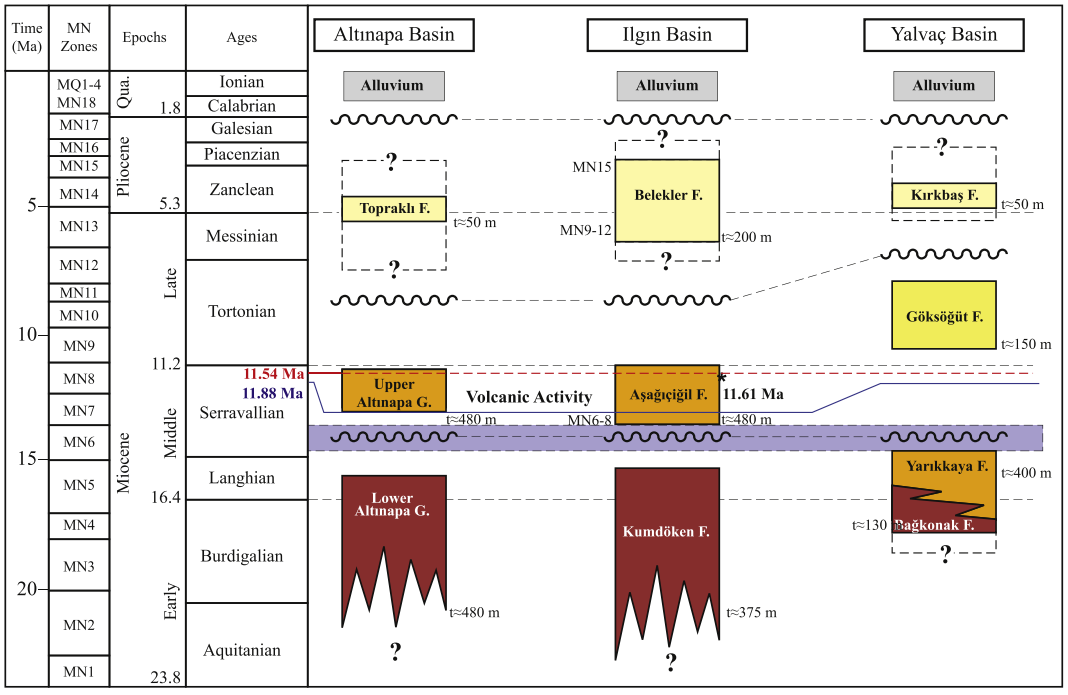

Fig. 12. Correlation of the unconformity bounded lithologic units of each basin. Note that the basic angular unconformity surface occured during Middle Miocene are correlated.

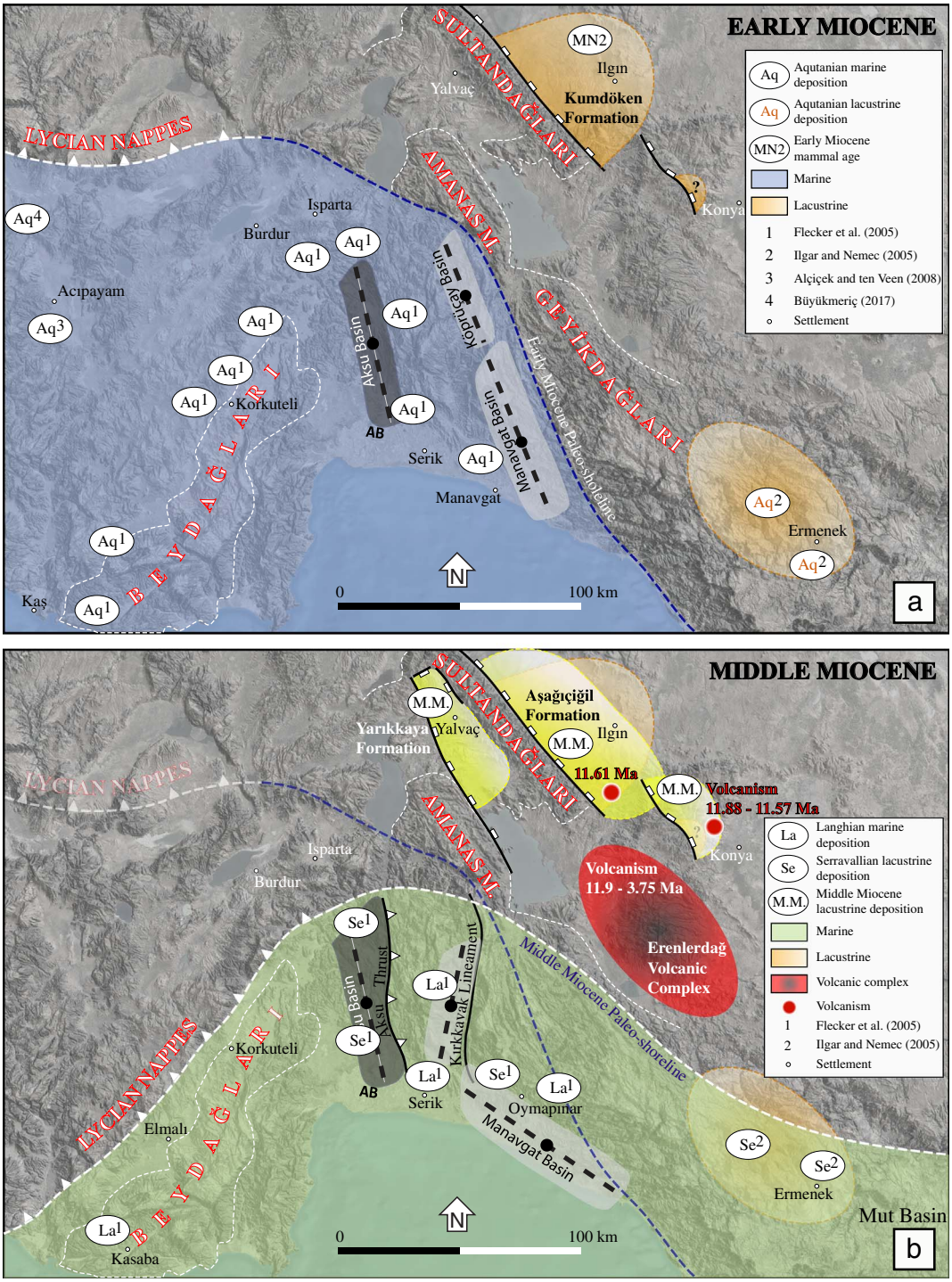

Fig. 13. Paleogeographic maps showing the Early and Middle Miocene shorelines and the continental basins in the SW Turkey (position of the Lycian Nappes adopted from Hayward 1984).

Antalya slab may have generated in Central Anatolia should be taken into account when aiming to explain Central Anatolian Plateau rise.

Acknowledgements

Research for this paper occurred within the context of the ÖYP research fund of Turkish Government (No: BAP-08-11-DPT.2002K120510), and was supported by TUBITAK (the Scientific and Technological Research Council of Turkey) project (Grant Number ÇAYDAG-111Y239). DJJvH acknowledges ERC Starting Grant number 306810 (SINK) and NWO VIDI grant 864.11.004. KK acknowledges NWO VIDI grant 864.12.005. AK thanks Hasan Kocatepe, Ayşe Kocatepe, Kemal Koç, Onur Öztepe, Murat Özkaptan, Erhan Gülyüz and Orhan Karaman for their help during fieldworks in 2008 and 2010.

Supplementary data to this article can be found online at http://dx.doi.org/10.1016/j.gloplacha.2017.09.001.

References

Aktuğ, B., Kaypak, B., Çelik, R.N., 2010. Source parametersfor the Mw = 6.6, 03 February 2002, Çay earthquake (Turkey) and afterschocks from GPS, Southeastern Turkey. J.

Seismol. 14, 445–456. http://dx.doi.org/10.1007/s10950-009-9174-y.
Angelier, J., 1979. Determination of mean principal direction of stress for a given fault population. Tectonophysics 56, T17–T26.
Angelier, J., 1990. Inversion of field data in fault tectonics to obtain the regional stress—III. A new rapid direct inversion method by analytical means. Geophys. J. Int. 103, 363–376.
Angelier, J., 1994. Fault slip analysis and paleostress reconstruction. In: Hancock, P.L. (Ed.), Continental deformation. Pergamon Press, Oxford, pp. 53–101.
Armijo, R., Carey, E., Cristernas, A., 1982. The inverse problem in microtectonics and the separation of tectonic phases. Tectonophy 82, 145–160.
Barka, A., Reilinger, R., Şaroğlu, F., Şengör, A.M.C., 1995. The Isparta angle: its importance in the neotectonics of the Eastern Mediterranean Region. Proc. Int. Earth Sci. Colloq. Aegean Reg. 1, 3–18.
Bartol, J., Govers, R., 2014. A single cause for uplift of the Central and Eastern Anatolian plateau? Tectonophysics 637 (C), 116–136. http://dx.doi.org/10.1016/j.tecto.2014.10.002.
Bassant, P., van Buchem, F.S.P., Strasser, A., Görür, N., 2005. The stratigraphic architecture and evolution of the Burdigalian carbonate–siliciclastic sedimentary systems of the Mut Basin, Turkey. Sediment. Geol. 173, 187–232.
Bektimuroğlu, O., 1978. Konya ili Ilgın ilçesi civarındaki kil yatakları hakkında ön rapor. M.T.A Rapor No: 6238. (in Turkish).
Besang, C., Eckhart, F.J., Harre, W., Kreuzer, G., Muller, P., 1977. Radiometrische Alterbestimmung am neogenen Eruptivgesteinen der Türkei. Geol. Jb. 25, 3–36.
Biryol, C.B., Beck, S.L., Zandt, G., Ozacar, A.A., 2011. Segmented African lithosphere beneath the Anatolian region inferred from teleseismic P-wave tomography. Geophys. J. Int. 184, 1037–1057.
Boray, A., Şaroğlu, F., Emre, Ö., 1985. Isparta büklümünün kuzey kesiminde D-B daralma için bazı veriler. Jeoloji Mühendisliği 23, 9–20.
Carey, E., Burinier, B., 1974. Analyse théorique et numérique d'un modèle mécanique élémentaire appliqué à l'étude d'une population de failes. Comptes Rendus Acadademie Science Paris D279, 891–894.
Çelik, Ö.F., Delaloyle, M.F., Feraud, G., 2006. Precise 40 Ar– 39 Ar ages from the metamorphic sole rocks of the Tauride Belt Ophiolites, southern Turkey: implications for the rapid cooling history. Geol. Mag. 143 (02), 213–227. http://dx.doi.org/10.1017/S0016756805001524.
Çiner, A., Karabiyikoglu, M., Monod, O., Deynoux, M., Tuzcu, S., 2008. Late Cenozoic sedimentary evolution of the Antalya Basin, Southern Turkey. Turk. J. Earth Sci. 17, 1–41.
Cipollari, P., Cosentino, D., Radeff, G., Schildgen, T.F., Faranda, C., Grossi, F., ... Echtler, H., 2013. Easternmost Mediterranean evidence of the Zanclean flooding event and subsequent surface uplift: Adana Basin, southern Turkey. Geol. Soc. Lond., Spec. Publ. 372 (1), 473–494. http://dx.doi.org/10.1144/SP372.5.
Colby, B.R., 1963. Fluvial sediments – a summary of source, transportation, deposition, and measurement of sediment discherge. In: United States Geological Survey Bulletin 1181A.
Cosentino, D., Schildgen, T.F., Cipollari, P., Faranda, C., Gliozzi, E., Hudackova, N., Lucifora, S., Strecker, M.R., 2012. Late Miocene surface uplift of the southern margin of the Central Anatolian Plateau, Central Taurides, Turkey. Geol. Soc. Am. Bull. 124 (1–2), 133–145. http://dx.doi.org/10.1130/B30466.1.
Çuhadar, G., 1977. Akarçay havzası Hidrojeolojik etüd Raporu, General Directorate of State Hydraulic Works (DSİ) Reports (Unpublished, in Turkish).
Darbas, G., Nazik, A., 2010. Micropaleontology and paleoecology of the Neogene sediments in the Adana Basin (South of Turkey). J. Asian Earth Sci. 39, 136–147.
Derman, A.S., Gürbüz, K., 2007. Nature, provenance and relationships of Early Miocene palaeovalley fills, northern Adana Basin, Turkey: their significance for sedimentby-passing on a carbonate shelf. Turk. J. Earth Sci. 16, 181–209.
Dokuz, A., Aydınçakır, E., Kandemir, R., Karslı, O., Siebel, W., Derman, A.S., Turan, M., 2017. Late Jurassic magmatism and stratigraphy in the eastern Sakarya zone, Turkey: evidence for the slab breakoff of paleotethyan oceanic lithosphere. J. Geol. 125 (1), 1–31. http://dx.doi.org/10.1086/689552.
Dunne, W.M., Hancock, P.L., 1994. Paleostress analysis of small-scale brittle structures. In: Hancock, P.L. (Ed.), Continental Deformation. Pergamon Press, Oxford, pp. 101–120.
Eren, Y., 1993. Eldes-Derbent-Tepeköy-Sögütözü Arasinin Jeolojisi. PhD Thesis. S.Ü. Fen Bil. Enst, Konya, Turkey, pp. 224.
Eren, Y., 1996. Ilgın-Sarayönü (Konya) güneyinde Bozdaglar Masifinin Yapısal Özellikleri. Geological Bulletin of Turkey 39, 49–64.
Ergin, M., Aktar, M., Özalaybey, S., Tapirdamaz, M.C., Selvi, O., Tarancioglu, A., 2009. A high-resolution aftershock seismicity image of the 2002 Sultandagi-Çay earthquake (Mw = 6.2), Turkey. J. Seismol. 13, 633–646.
Eriş, K.K., Bassant, P., Ülgen, U.B., 2005. Tectono-stratigraphic evolution of an Early Miocene incised valley-fill (Derinçay Formation) in the Mut Basin, Southern Turkey. Sediment. Geol. 173, 151–185.
Esirtgen, T., 2014. Tectono-sedimentary evolution of Bucakkisla region (SW Karaman) in central Taurides. Bull. Min. Res. Exp. 148, 19–42.
Etchecopar, A., Vasseur, D., Daignières, M., 1981. An inverse problem in microtectonics for determination of stress tensors from faults striation analysis. J. Struct. Geol. 3, 51–65.
Faccenna, C., Bellier, O., Martinod, J., Piromallo, C., Regard, V., 2006. Slab detachment beneath eastern Anatolia: a possible cause for the formation of the North Anatolian Fault. Earth Planet. Sci. Lett. 242, 85–97.
Fernandez-Blanco, D., 2014. Evolution of Orogenic Plateaus at Subduction Zones: Sinking and Raising the Southern Margin of the Central Anatolian Plateau. PhD Thesis. VU University Amsterdam978-90-9028673-0 226 p.
Gans, C.R., Beck, S.L., Zandt, G., Biryol, C.B., Ozacar, A.A., 2009. Detecting the limit of slab break-off in central Turkey: new high-resolution Pn tomography results. Geophys. J. Int. 179, 1566–1572.
Glennie, K.W., 1970. Desert Sedimentary Environments. Elsevier, Amstredam, pp. 148.
Göğer, E., Kıral, K., 1969. Kızılören Dolayının Jeolojisi. M.T.A. Rappor, pp. 5204.
Görür, N., Oktay, F.Y., Seymen, I., Şengör, A.M.C., 1984. Paleotectonic evolution of Tuzgölü basin complex, Central Turkey. In: Dixon, J.E., Robertson, A.H.F. (Eds.), The Geological Evolution of the Eastern Mediterranean. Spec. Publ. Geol. Soc Vol. 17. Blackwell Scientific, London, pp. 81–96.
Govers, R., Fichtner, A., 2016. Signature of slab fragmentation beneath Anatolia from full-waveform tomography. Earth Planet. Sci. Lett. 450 (C), 10–19. http://dx.doi.org/10.1016/j.epsl.2016.06.014.
Granot, R., 2016. Palaeozoic oceanic crust preserved beneath the eastern Mediterranean. Nat. Geosci. 9, 701–705. http://dx.doi.org/10.1038/ngeo2784.
Gül, M., 2007. Effects of antecedent topography on reefal carbonate deposition: early–middle Miocene of the Adana Basin, S Turkey. J. Asian Earth Sci. 31, 18–34.
Gürer, D., van Hinsbergen, D., Maţenco, L., Corfu, F., Cascella, A., 2016. Kinematics of a former oceanic plate of the Neotethys revealed by deformation in the Ulukışla basin (Turkey). Tectonics 35, 2385–2416. http://dx.doi.org/10.1002/(ISSN)1944-9194.
Hayward, A.B., 1984. Miocene clastic sedimentation related to the emplacement of the Lycian Nappes and the Antalya Complex SW Turkey. Geol. Soc. Lond. Spec. Publ. 17, 287–300.
Huang, Q., Angelier, J., 1989. Inversion of field data in fault tectonics to obtain the regional stress-II. Using conjugate fault sets within heterogeneous families for computing palaeostress axes. Geophys. J. 96, 139–149.
Hüseyinca, M.Y., Eren, Y., 2007. Ilgın (Konya) kuzeyinin stratigrafisi ve tektonik evrimi. Selçuk Üniv. Mühendislik Mimarlık Fakül. Derg. 22, 1–2.
Ilgar, A., Nemec, W., 2005. Early Miocene lacustrine deposits and sequence stratigraphy of the Ermenek Basin, Central Taurides, Turkey. Sediment. Geol. 173 (1), 233–275.
Janson, X., van Buchem, F.S.P., Dromart, G., Eichenseer, H.T., Dellamonics, X., Boichard, R., Bonnaffe, F., Eberli, G.P., 2010. Architecture and facies differentiation within a Middle Miocene carbonate platform, Ermenek, Mut Basin, southern Turkey. In: van Buchem, F.S.P., Gerdes, K.D., Esteban, M. (Eds.), Mesozoic and Cenozoic Carbonate Systems of the Mediterranean and the Middle East: Stratigraphic and Diagenetic Reference Models: Geological Society. Special Publications, London, pp. 265–290.
Kalyoncuoğlu, Ü.Y., Elitok, Ö., Dolmaz, M.N., Anadolu, N.C., 2011. Geophysical and geological imprints of southern Neotethyan subduction between Cyprus and the Isparta angle, SW Turkey. J. Geodyn. 52 (1), 70–82. http://dx.doi.org/10.1016/j.jog.2010.12.001.
Karabıyıkoğlu, M., Tuzcu, S., Çiner, A., Deynoux, M., Örçen, S., Hakyemez, A., 2005. Facies and environmental setting of the Miocene coral reefs in the late-orogenic fill of the Antalya Basin, western Taurides, Turkey: implications for tectonic control and sea-level changes. Sediment. Geol. 173, 345–371.
Karayiğit, A.I., Akgün, F., Gayer, R.A., Temel, A., 1999. Quality, palynology, and paleoenvironmental interpretation of the Ilgın lignite, Turkey. International Journal of Coal Geology 38, 219–236.
Kaymakci, N., Özçelik, Y., White, S.H., van Dijk, P.M., 2009. Tectono-Stratigraphy of the Çankiri Basin: late Cretaceous to early Miocene evolution of the Neotethyan suture zone in Turkey. In: Edwards, M.A., Govers, R. (Eds.), van Hinsbergen, D.J.J. Geological Society of London Special Publication, Collision and Collapse at the Africa-Arabia-Eurasia subduction zone, pp. 67–106.
Kaymakci, N., Inceöz, M., Ertepınar, P., Koç, A., 2010. Late cretaceous to recent kinematics of SE Anatolia (Turkey). Geol. Soc. Lond., Spec. Publ. 340, 409–435.
Keller, J., Jung, D., Burgath, K., Wolff, F., 1977. Geologie und Petrologie des Neogenen Kalkalkalivulkanismus von Konya (Erenler Dağı, Alacadağ Massiv, Zentral Anatolian). Geologisches Jahrbuch, B. 25, 37–117.
Khair, K., Tsokas, G.N., 1999. Nature of the Levantine (eastern Mediterranean) crust from multiple-source Werner deconvolution of Bouguer gravity anomalies. J. Geophys. Res. 104, 25469–25478.
Kissel, C., Laj, C., 1988. The tertiary geodynamical evolution of the Aegean arc: a paleomagnetic reconstruction. Tectonophysics 146 (1–4), 183–201.
Kissel, C., Poisson, A., 1987. Étude paléomagnetique préliminaire des formations cénozoïques des Bey Daglari (Taurides occidentales, Turquie). Comptes rendus de l'Académie des sciences. Série 2, Mécanique, Physique, Chimie, Sciences de l'univers, Sciences de la Terre 304 (8), 343–348.
Koç, A., Kaymakci, N., van Hinsbergen, D.J.J., Kuiper, K.F., Vissers, R.L.M., 2012. Tectono-sedimentary evolution and geochronology of the middle Miocene Altınapa Basin, and implications for the late Cenozoic uplift history of the Taurides, southern Turkey. Tectonophysics 532-535, 134–155.
Koç, A., Kaymakci, N., Van Hinsbergen, D.J., Vissers, R.L.M., 2016a. A Miocene onset of the modern extensional regime in the Isparta Angle: constraints from the Yalvaç Basin (southwest Turkey). Int. J. Earth Sci. 105 (1), 369–398.
Koç, A., van Hinsbergen, D.J., Kaymakci, N., Langereis, C.G., 2016b. Late Neogene orocolinal bending in the central Taurides: a record of terminal eastward subduction in southern Turkey? Earth Planet. Sci. Lett. 434, 75–90.
Koçyiğit, A., 1984. Intra-plate neotectonic development in southwestern Turkey and adjacent areas. Bull. Geol. Soc. Turk. 27, 1–16.
Koçyiğit, A., Özacar, A.A., 2003. Extensional Neotectonic regime through the NE edge of the outer Isparta angle, SW Turkey: New field and seismic data. Turk. J. Earth Sci. 12, 67–90.
Koçyiğit, A., Ünay, E., Saraç, G., 2000. Episodic graben formation and extensional neotectonic regime in west central Anatolia and the Isparta Angle: a case study in the Akşehir-Afyon Graben, Turkey. Geol. Soc. Lond., Spec. Publ. 173, 405–421.
Koppers, A.A.P., 2002. ArArCALC-software for 40Ar/39Ar age calculations. Comput. Geosci. 28, 605–619.
Krijgsman, W., Duermeijer, C.E., Langereis, C.G., de Bruijn, H., Saraç, G., Andriessen, P.A.M., 1996. Magnetic polarity stratigraphy of late Oligocene to middle Miocene mammal-bearing localities in Central Anatolia (Turkey). Newsl. Stratigr. 34, 13–29.

Kuiper, K.F., Deino, A.L., Hilgen, F.J., Krijgsman, W., Renne, P.R., Wijbrans, J.R., 2008. Synchronizing rock clocks of earth history. Science 320, 500–504.
Lahn, E., 1945. Batı Toros göllerinin jeomorfolojisi. M.T.A Dergisi 2 (34), 387–400.
Lüdecke, T., Mikes, T., Rojay, B., Cosca, M.A., Mulch, A., 2013. Stable isotope-based reconstruction of Oligo-Miocene paleoenvironment and paleohydrology of Central Anatolian lake basins (Turkey). Turk. J. Earth Sci. 22, 1–28. http://dx.doi.org/10.3906/yer-1207-11.
van der Meer, D.G., van Hinsbergen, D.J., Spakman, W., 2017. The Atlas of the Underworld: a catalogue of slab remnants in the mantle imaged by seismic tomography, and their geological interpretation. Tectonophysics (v. submitted).
Meijers, M.J.M., Kaymakci, N., van Hinsbergen, D.J.J., Langereis, C.G., Stephenson, R.A., Hippolyte, J.-C., 2010. Late Cretaceous to Paleocene oroclinal bending in the Central Pontides (Turkey). Tectonics 29, TC4016. http://dx.doi.org/10.1029/2009TC002620.
Meijers, M.J.M., Strauss, B.E., Özkaptan, M., Feinberg, J.M., Mulch, A., Whitney, D.L., Kaymakcı, N., 2016. Age and paleoenvironmental reconstruction of partially remagnetized lacustrine sedimentary rocks (Oligocene Aktoprak basin, central Anatolia, Turkey). Geochem. Geophys. Geosyst. 17 (3), 914–939. http://dx.doi.org/10.1002/2015GC006209.
Mein, P., 1999. European Miocene mammal biochronology. Pp. 25–38 In: Rössner, G.E., Heissig, K. (Eds.), The Miocene Land Mammals of Europe. Verlag Dr. Friedrich Pfeil, Munich (515 pp).
Miall, A.D., 1996. The Geology of Fluvial Deposits, Sedimentary Facies. Basin Analysis and Petroleum Geology. Springer, Berlin, pp. 582.
Miall, A.D., Smith, N.D., 1989. Rivers and their deposits. Soc. Econ, Paleont And Mineral (Tulsa, Oklahoma).
Morris, A., Robertson, A.H.F., 1993. Miocene remagnetisation of carbonate platform and Antalya Complex units within the Isparta Angle, SW Turkey. Tectonophy 220, 243–266.
Nier, A.O., 1950. A redetermination of the relative abundances of the isotopes of Carbon, Nitrogen, Oxygen, Argon, and Potassium. Phys. Rev. 77, 789.
Okay, A.I., Sunal, G., Tüysüz, O., Sherlock, S., Keskin, M., Kylander-Clark, A.R.C., 2013. Low-pressure-high-temperature metamorphism during extension in a Jurassic magmatic arc, Central Pontides, Turkey. J. Metamorph. Geol. 32 (1), 49–69. http://dx.doi.org/10.1111/jmg.12058.
Özcan, A., Göncüoğlu, M.C., Turhan, N., Şentürk, K., Uysal, S., Isik, A., 1990. Konya-Kadınhanı-Ilgın Dolayinin Temel Jeolojisi. M.T.A. Rappor 9535.
Özdamar, S., Roden, M.F., Esenli, F., UZ, B., Wampler, J.M., 2012. Geochemical features and K-Ar age data from metadetrital rocks and high-K metasomatized metarhyolites in the Afyon- Bolkardag zone (Ilgin-Konya), SW Turkey. N. Jb. Miner. Abh 189 (2), 155–176. http://dx.doi.org/10.1127/0077-7757/2012/0216.
Özdamar, Ş., Billor, M.Z., Sunal, G., Esenli, F., Roden, M.F., 2013. First U–Pb SHRIMP zircon and 40Ar/39Ar ages of metarhyolites from the Afyon–Bolkardag zone, SW Turkey: implications for the rifting and closure of the Neo-Tethys. Gondwana Res. 24 (1), 377–391. http://dx.doi.org/10.1016/j.gr.2012.10.006.
Özkan, A.M., 1998. Konya Batisindaki Neojen Çökellerinin Stratigrafisi ve Sedimantolojisi. PhD Thesis. S.Ü. Fen Bil. Enst., Konya, Türkey (208 pp).
Özkan, A.M., Söğüt, A.R., 1999. Dilekçi (Konya batısı) çevresindeki Neojen çökellerinin stratigrafisi. Journal of Engineering Science 5, 1131–1138.
Parlak, O., 2016. The tauride ophiolites of Anatolia (Turkey): a review. J. Earth Sci. 27 (6), 901–934. http://dx.doi.org/10.1007/s12583-016-0679-3.
Parlak, O., Karaoğlan, F., Rızaoğlu, T., Klötzli, U., Koller, F., Billor, Z., 2013. U-Pb and 40Ar-39Ar geochronology of the ophiolites and granitoids from the Tauride belt: implications for the evolution of the Inner Tauride suture. J. Geodyn. 65, 22–37. http://dx.doi.org/10.1016/j.jog.2012.06.012.
Plunder, A., Agard, P., Chopin, C., Pourteau, A., Okay, A.I., 2015. Accretion, underplating and exhumation along a subduction interface: from subduction initiation to continental subduction (Tavşanlı zone, W. Turkey). Lithos 226, 233–254. http://dx.doi.org/10.1016/j.lithos.2015.01.007.
Poisson, A., Wernli, R., Sagular, E.K., Temiz, H., 2003. New data concerning the age of the Aksu thrust in the south ofthe Aksu valley, Isparta Angle (SW Turkey): consequences for the Antalya Basin and the Eastern Mediterranean. Geol. J. 38, 311–327.
Pourteau, A., Candan, O., Oberhänsli, R., 2010. High-pressure metasediments in central Turkey: constraints on the Neotethyan closure history. Tectonics 29, TC5004. http://dx.doi.org/10.1029/2009TC002650.
Pourteau, P., Bousquet, R., Vidal, O., Plunder, A., Duesterhoeft, E., Candan, O., Oberhansli, R., 2014. Multistage growth of Fe-Mg-carpholite and Fe-Mg-chloritoid, from field evidence to thermodynamic modelling. Contrib. Mineral. Petrol. 168, 1090. http://dx.doi.org/10.1007/s00410-014-1090-7.
Radeff, G., Cosentino, D., Cipollari, P., Schildgen, T.F., Iadanza, A., Strecker, M., Darbas, G., Gurbuz, K., 2016. Stratigraphic architecture of the upper Messinian deposits of the Adana Basin (Southern Turkey): implications for the Messinian salinity crisis and the Taurus petroleum system. Ital. J. Geosci. 135 (3), 408–424. http://dx.doi.org/10.3301/IJG.2015.18.
Radeff, G., Schildgen, T.F., Cosentino, D., Strecker, M.R., Cipollari, P., Darbas, G., Gurbuz, K., 2017. Sedimentary evidence for late Messinian uplift of the SE margin of the Central Anatolian Plateau: Adana Basin, southern Turkey. Basin Res. 29, 488–514. http://dx.doi.org/10.1111/bre.12159.
Saraç, G., 2001. Türkiye omurgalı fosil yatakları, Maden Tetkik ve Arama Genel Müdürlüğü Raporu (unpublished). (Ankara).
Şaroğlu, F., Emre, Ö., Boray, A., 1987. Türkiye'nin Diri Fayları ve Depremselliği [Seismicity and Active Faults of Turkey]. General Directorate of Mineral Research and Exploration (MTA) Report No. 8174.
Schemmel, F., Mikes, T., Rojay, B., Mulch, A., 2013. The impact of topography on isotopes in precipitation across the Central Anatolian Plateau (Turkey). Am. J. Sci. 313 (2), 61–80. http://dx.doi.org/10.2475/02.2013.01.
Schildgen, T.F., Cosentino, D., Bookhagen, B., Niedermann, S., Yıldırım, C., Echtler, H., Wittmann, H., Strecker, M.R., 2012a. Multi-phased uplift of the southern margin of the Central Anatolian plateau, Turkey: A record of tectonic and upper mantle processes. Earth Planet. Sci. Lett. 317–318, 85–95. http://dx.doi.org/10.1016/j.epsl.2011.12.003.
Schildgen, T.F., Cosentino, D., Caruso, A., Buchwaldt, R., Yıldırım, C., Bowring, S.A., Rojay, B., Echtler, H., Strecker, M.R., 2012b. Surface expression of Eastern Mediterranean slab dynamics: Neogene topographic and structural evolution of the SW margin of the Central Anatolian Plateau, Turkey. Tectonics 31 (2). http://dx.doi.org/10.1029/2011TC003021.
Schildgen, T.F., Yıldırım, C., Cosentino, D., Strecker, M.R., 2014. Linking slab break-off, Hellenic trench retreat, and uplift of the Central and Eastern Anatolian plateaus. Earth Sci. Rev. 128 (C), 147–168. http://dx.doi.org/10.1016/j.earscirev.2013.11.006.
Şenel, M., 2002. Geological Map of Turkey, Konya (No.14): Ankara, Turkey, Maden Tetkik ve Arama Genel Müdürlüğü (MTA), Scale 1;500,000, 1 Sheet.
Şengör, A.M.C., Yilmaz, Y., 1981. Tethyan evolution of Turkey: a plate tectonic approach. Tectonophysics 75, 181–241.
Steiger, R.H., Jäger, E., 1977. Subcommission on geochemistry: convention on the use of decay constants in geo- and cosmochronology. Earth Planet. Sci. Lett. 36, 359–362.
Steininger, F., 1999. Chronostratigraphy, geochronology and biochronology of the Miocene "European land mammal mega-zones (ELMMZ)" and the Miocene "mammal zones (MN-zones)". Pp. 9–24. In: Rössner, G.E., Heissig, K (Eds.), The Miocene Land Mammals of Europe. Munich, Verlag Dr. Friedrich Pfeil, (515 pp).
Talbot, M.R., Allen, P.A., 1996. Lakes. In reading In: H.G. (Ed.), Sedimentary environments: Process, Facies, Stratigraphy. Blackwell Science Ltd, Oxford, pp. 83–124.
Tatar, O., Gürsoy, H., Piper, J.D.A., 2002. Differential neotectonic rotations in Anatolia and the Tauride Arc: palaeomagnetic investigation of the Erenlerdağ Volcanic Complex and Isparta volcanic district, south-central Turkey. J. Geol. Soc. Lond. 159, 281–294.
Taymaz, T., Tan, O., 2001. Source parameters of June 6, 2000 Orta-Çankırı (Mw = 6.0) and December 15, 2000 Sultandağ-Akşehir (Mw = 6.0) earthquakes obtained from inversion of teleseismic P and SH body-waveforms. In: Scientific Activities 2001 Symposia Book, İstanbul Technical University, Faculty of Mines, May 8, 2001, Istanbul, Turkey, pp. 96–107.
Taymaz, T., Tan, O., Yolsal, S., 2004. Seismotectonics of western Turkey: a synthesis of source parameters and rupture histories of Recent earthquakes. Eos Trans. AGU 85, 47.
Temel, A., Gündogdu, M.N., Gourgaud, A., 1998. Petrological and geochemical characteristic of Cenozoic high-K calcalkaline volcanism in Konya, Central Anatolia, Turkey. J. Volcanol. Geotherm. Res. 85, 327–354.
Ten Veen, J.T., Boulton, S.J., Alçiçek, M.C., 2009. From palaeotectonics to neotectonics in the Neotethys realm: the importance of kinematic decoupling and inherited structural grain in SW Anatolia (Turkey). Tectonophysics 473 (1), 261–281.
Tüfekçi, K., 1987. Ilgın Gölü ve Dolayının Jeomorfolojisi. Ankara Üniversitesi, Fen Bilimleri Enstitüsü, Ankara Yük. Lis. Tezi. (Unpublished, In Turkish).
Umut, M., Karabıyıkoğlu, M., Saraç, G., Bulut, V., Demirci, A.R., Erkan, M., Kurt, Z., Metin, S., Özgönül, E., 1987. Tuzlukçu-Ilgın-Doğanbey (Konya ili) ve dolayının jeolojisi. M.T.A. Rapor No: 8246. (Unpublished).
van Hinsbergen, D.J.J., Dekkers, M.J., Koç, A., 2010a. Testing Miocene remagnetization of Bey Dağları: timing and amount of Neogene rotations in SW Turkey. Turk. J. Earth Sci. 19, 123–156.
van Hinsbergen, D.J.J., Kaymakci, N., Spakman, W., Torsvik, T.H., 2010b. Reconciling the geological history of western Turkey with plate circuits and mantle tomography. Earth Planet. Sci. Lett. 297, 674–686.
van Hinsbergen, D.J.J., Peters, K., Maffione, M., Spakman, W., Guilmette, C., Thieulot, C., ... Kaymakcı, N., 2015. Dynamics of intraoceanic subduction initiation: 2. Suprasubduction zone ophiolite formation and metamorphic sole exhumation in context of absolute plate motions. Geochem. Geophys. Geosyst. 16, 1771–1785.
van Hinsbergen, D.J., Maffione, M., Plunder, A., Kaymakci, N., Ganerød, M., Hendriks, B.W.H., ... Vissers, R.L.M., 2016. Tectonic evolution and paleogeography of the Kırşehir Block and the Central Anatolian Ophiolites, Turkey. Tectonics 35, 983–1014. http://dx.doi.org/10.1002/(ISSN)1944-9194.
Walker, R.G., 1967. Turbidite sedimentary structures and their relationship to proximal and distal depositional environments. J. Sediment. Petrol. 37, 25–43.
Walker, R.E., James, N.P., 1992. Facies Models: Response to Sea-level Change. Geol. Ass. Can. Waterloo, Ontario. pp. 238.
Wallace, R.E., 1951. Geometry of shearing stress and relation to faulting. J. Geol. 59, 118–130.
Wedding, H., 1954. Yalvaç'ın şimalinde Yarıkkaya linyit zuhuru hakkında rapor: MTA Rapor No: 2200. (Unpublished).
Yağmurlu, F., 1991a. Stratigraphy and depositional environments of Yalvaç-Yarıkkaya Neogene basin, SW-Anatolia. Geological Bulletin of Turkey 34, 9–19.
Yağmurlu, F., 1991b. Yalvaç-Yarikkaya Neojen havzasinin tektono-sedimanter özellikleri ve yapisal evrimi. M.T.A. Dergisi, Sayi 112, 1–13.
Yalınız, M.K., Göncüoğlu, M.C., 1998. General Geological characteristics and distribution of the central Anatolian Ophiolites. Yerbilimleri 20, 19–30.
Yamaji, A., 2000. Multiple inverse method: a new technique to separate stresses from heteregenous fault-slip data. J. Struct. Geol. 22, 441–452.
Yetiş, C., 1988. Reorganization of the Tertiary stratigraphy in the Adana basin, southern Turkey. Newsl. Stratigr. 20, 43–58.
Yilmaz, Y., 1993. New evidence and model on the evolution of the Southeast Anatolia Orogen. Geol. Soc. Am. Bull. 105, 251–271.